Institute for Energy

ENIQ 2nd PILOT STUDY – DEFECT ASSESSMENT AND DESTRUCTIVE EXAMINATION REPORT

ENIQ Report nr. 32

ENIQ

European Network for Inspection and Qualification

EUROPEAN COMMISSION
DIRECTORATE-GENERAL
Joint Research Centre
EUR 22908 EN

Mission of the Institute for Energy
The Institute for Energy provides scientific and technical support for the conception, development, implementation and monitoring of community policies related to energy. Special emphasis is given to the security of energy supply and to sustainable and safe energy production.

European Commission
Directorate-General Joint Research Centre (DG JRC)
http://www.jrc.ec.europa.eu/

Institute for Energy, Petten (the Netherlands)
http://ie.jrc.ec.europa.eu/

Contact details:
Arne Eriksson
Tel: +31 (0) 224 56 5383
E-mail: arne.eriksson@jrc.nl

Legal Notice

EUR 22908 EN
ISSN 1018-5593
Luxembourg: Office for Official Publications of the European Communities

Printed in the Netherlands

European Commission
Directorate General Joint Research Centre
Institute for Energy
Petten, The Netherlands

ENIQ 2nd PILOT STUDY – DEFECT ASSESSMENT AND DESTRUCTIVE EXAMINATION REPORT

November 2007 ***ENIQ Report nr. 32*** ***EUR 22908 EN***

Approved for publication by the ENIQ Task Group for Qualification

Documents published by ENIQ, the European Network for Inspection and Qualification, belong to one of the following 3 types:

Type 1 – **Consensus Document**
A *consensus document* contains harmonised principles, methodologies, approaches and procedures, and stresses the degree of harmonisation on the subject among ENIQ members.

Type 2 – **Position/Discussion Document**
A *position/discussion document* may contain compilations of ideas, expressions of opinion, reviews of practices, or conclusions and recommendations from technical projects.

Type 3 – **Technical Report**
A *technical report* is a document containing results of investigations, compilations of data, reviews and procedures without expressing any specific opinion or valuation on behalf of ENIQ.

The present document "ENIQ 2nd Pilot Study – Defect Assessment and Destructive Examination Report" (ENIQ Report nr. 32) is a Type 3 document.

Foreword

The present work is one outcome of the activities of the ENIQ Task Group for Qualification (TGQ) on the ENIQ 2nd Pilot Study.

ENIQ, the European Network for Inspection and Qualification, is driven by the nuclear utilities in the European Union and Switzerland and managed by the European Commission's Joint Research Centre (JRC). It is active in the field of in-service inspection (ISI) of nuclear power plants by non-destructive testing (NDT), and works mainly in the areas of qualification of NDT systems and risk-informed in-service inspection (RI-ISI). This technical work is performed in two task groups: TG Qualification and TG Risk.

A key achievement of ENIQ has been the issue of a European Qualification Methodology Document, which has been widely adopted across Europe[1]. This document defines an approach to the qualification of inspection procedures, equipment and personnel based on a combination of technical justification (TJ) and test piece trials (open or blind). The TJ is a crucial element in the ENIQ approach, containing evidence justifying that the proposed inspection will meet its objectives in terms of defect detection and sizing capability. A qualification body reviews the TJ and the results of any test piece trials and it issues the qualification certificates.

ENIQ has previously conducted a pilot study to assess the feasibility of the ENIQ Methodology in practice[2]. This first pilot study was successful but, because the component chosen for the study was an austenitic weld, could not fully explore the use of TJs. This is because techniques such as mathematical modelling, at the time of the study, tended to be applicable only to isotropic materials. Assessment of the inspectability of austenitic welds usually requires the use of test pieces with the same metallurgical structure. Accordingly, ENIQ decided to conduct a second pilot study using a ferritic nozzle to shell weld.

The main objective of the second pilot study was to show how to fully exploit the potential of TJs in the qualification of inspection procedures and thereby reduce the number of test piece trials on full-scale components[3,4]. As the subject of the study, a ferritic BWR-type nozzle to shell weld was selected. A TJ was produced, partly relying on modelling, to predict whether a designated ultrasonic inspection would be successful in detecting the specified defects[5]. In parallel, a test piece with deliberately introduced defects was fabricated and inspected with the inspection system specified in the TJ. The test piece was destructively examined following completion of all inspection work[6,7,8]. This report summarises the results of the destructive examinations.

This study has been conducted within the frame of ENIQ Task Group for Qualification. The contributors, in alphabetical order, are listed below:

I Atkinson	Kande, United Kingdom
J-A Berglund	Ringhals NPP, Sweden
R Booler	Serco, United Kingdom, Chairman of Task Group Qualification
R Chapman	British Energy, United Kingdom
Ph Dombret	Suez-Tractebel, Belgium
A Eriksson	Directorate General JRC, European Commission
L Horáček	NRI- Řež, Czech Republic
A Jonsson	Forsmark NPP, Sweden
P Kelsey	Rolls-Royce Marine Power, United Kingdom
P Krebs	Engineer Consulting, Switzerland
L Le Ber	M2M, France
B Neundorf	Vattenfall Europe Nuclear Energy, Germany

T Seldis	Directorate General JRC, European Commission, Co-chairman of Task Group Qualification
H Söderstrand	SQC Swedish NDT Qualification Centre, Sweden
C Waites	Serco, United Kingdom
A Walker	Rolls-Royce Marine Power, United Kingdom
J Whittle	John Whittle & Associates, United Kingdom,
H Wirdelius	Chalmers University of Technology, Sweden

This ENIQ Type 3 document was approved for publication by the ENIQ Task Group for Qualification.

Disclaimer

ENIQ is a network of interested European organisations developing methodologies for inspection qualification and risk-informed in-service inspection. ENIQ does not review, endorse or accredit individual qualifications carried out on plant belonging to member utilities, nor does ENIQ operate an accreditation system for Qualification Bodies. Statements by utilities and others that a specific qualification is compliant with the ENIQ methodology should not therefore be taken as implying approval or endorsement of that qualification by the ENIQ network as a whole.

TABLE OF CONTENTS

1. INTRODUCTION

This report is part of the ENIQ 2nd Pilot Study, conducted by ENIQ Task Group Qualification, which investigated the role of technical justifications within the inspection qualification process. As the subject of the study, a ferritic BWR-type nozzle to shell weld was selected. This document compiles the results of the defect assessment and destructive examination carried out to determine the true dimensions and orientations of the defects, which have been implanted into the ENIQ nozzle assembly 21.

Two different fabrication techniques have been used to implant the defects. Both surface breaking and near surface defects were produced by spark erosion using an electrode with a sharp tip. These are so-called PISC type A defects, and silica based replicas were taken on each defect after manufacturing. The silica based replicas were examined by the JRC, Institute for Energy in Petten. The second group of defects are located on the weld fusion faces and are embedded in the base material. These sidewall lack of fusion defects, which were produced by means of the so-called coupon technique, have been destructively examined by the Nuclear Research Institute (NRI) Řež.

2. COMPONENT AND DEFECTS

2.1 COMPONENT INVOLVED

The component chosen for the pilot study was a ferritic nozzle to shell weld resembling those found in the reactor pressure vessels of BWRs as shown in Figure 1. In what follows, the clad surface of the test piece is referred to as the inner or inside surface because it corresponds to what would be the inside surface of a real pressure vessel. The other surface of the shell is referred to as the outer or outside surface for the same reason. The plate representing the RPV shell was clad using a 2-layer strip process with the strips parallel to what would be the axial direction in a real vessel. This does not correlate with the normal direction in a real vessel and was chosen to simplify the fabrication of the test piece. It does not affect the outcome of the pilot study because defects were inserted around the circumference of the weld so that inspecting probes were scanned over the full range of angles in relation to the cladding direction. The clad surface was hand ground after welding.

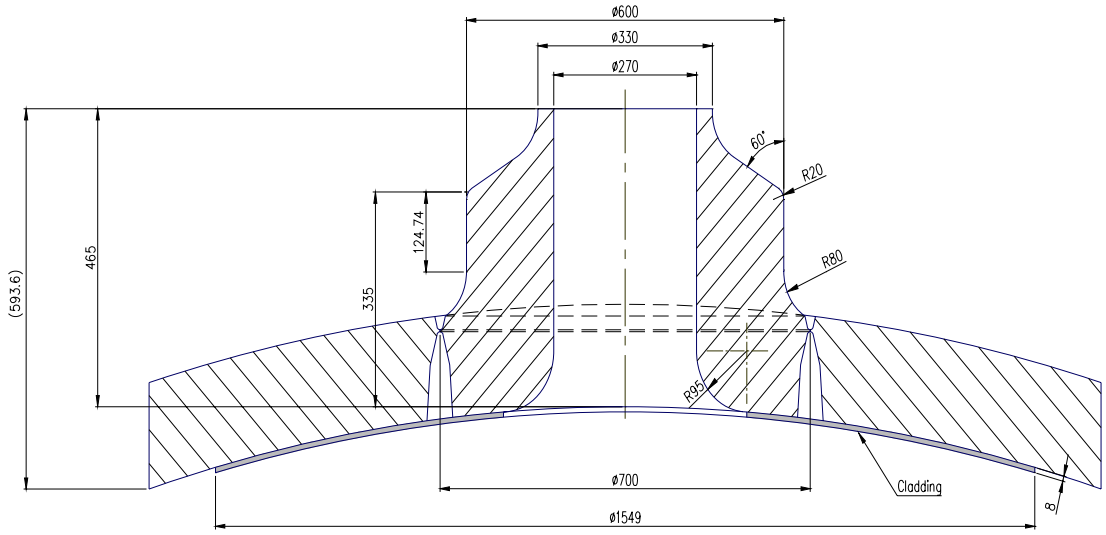

Vessel diameter	Inner radius	Weld prep. angle	Shell thickn.	Nozzle diam.	Shell weld diam.	Nozzle surface to shell weld centre
~6400	95	4	~160	270	700	215

Figure 1 – Diagram of the nozzle showing dimensions (in mm)

2.2 DEFECTS

The defect specification was as follows:

- Inspection volume is the third of the material nearest the inside surface in either the weld or heat-affected zone which is 10 mm on either side of the weld fusion line.
- All defects are smooth with surface roughness less than 6.3 µm Ra.
- Lack of fusion defects are on the fusion lines and are tilted at the same angle with zero skew.
- Defects at the surface or cladding interface are tilted up to ±20º from normal to the surface and skewed up to ±5º from the weld run direction.
- The qualification defect size is 15 mm in through-wall extent and 30 mm long.

The defects that were inserted into the test piece are listed in Table 1. Some defects smaller than the qualification size were included to explore inspection sensitivity at lower sizes. As outlined above, the inserted defects were in three groups:

Surface breaking defects: These are defects at the inside surface of the test piece over the nozzle weld having their tips either in the cladding or in the weld material underneath. They were produced by spark erosion using an electrode with a sharp tip and have tip radii of less than 40 µm. These are so-called PISC type A defects.

Near surface defects: These are defects produced by the same process as that above that were surface breaking prior to cladding. They therefore simulate cracks growing from the cladding interface.

Sidewall lack of fusion defects: These are the defects associated with the coupons on the fusion faces. They are oriented at the fusion face angle and are all embedded.

No.	Type of defect	Fabrication technique	Height [mm]	Length [mm]	Ligament [mm]	Position	Tilt [deg]	Skew [deg]
1	Near surface crack	PISC type A defects	5	20	8	Centreline	0	0
2	Surface crack		5	20	0	Centreline	0	0
3	Surface crack		5	20	0	Centreline	10	5
4	Surface crack		10	30	0	Centreline	10	0
5	Surface crack		10	30	0	Centreline	0	0
6	Surface crack		15	60	0	Centreline	0	5
7	Surface crack		15	60	0	Centreline	20	5
8	Near surface crack		5	20	8	Centreline	10	5
9	Near surface crack		10	40	8	Fusion line	4	0
10	Near surface crack		10	40	8	Fusion line	20	5
11	Near surface crack		15	60	8	Fusion line	10	0
12	Near surface crack		15	60	8	Fusion line	0	5
13	Sidewall lack of fusion	Coupon technique	10	20	10	Fusion line	4	0
14	Sidewall lack of fusion		15	30	20	Fusion line	4	0
15	Sidewall lack of fusion		15	30	30	Fusion line	4	0
16	Sidewall lack of fusion		5	50	10	Fusion line	4	0
17	Sidewall lack of fusion		5	60	15	Fusion line	4	0

Table 1 – Test piece defects

3. SUMMARY OF RESULTS

3.1 SURFACE BREAKING DEFECTS

This section presents the result of the investigation of the surface breaking defects. All 6 defects, numbered from 2 to 7, were inserted by spark erosion using electrodes shaped to produce sharp tips – so called PISC Type A defects. After manufacturing silica based replicas were taken on each defect, which were then investigated by the JRC, Institute for Energy in Petten.

Dimensions

Defect dimensions, length and height, have been measured directly on the replicas under a microscope. The results are reported in Table 2, together with design data for the defects. The maximum departure from intended defect length and height sizes was found to be equal or less than 0.1 mm and 0.4 mm, respectively. The through-wall extent values are reported as well, taken into account the effective tilt of the defects. The effective tilt is measured relative to the surface normal, which varies according to the defect location, due to the curvature of the shell plate.

Crack tip geometry and opening angle

The investigation of replicas under microscope has confirmed that the crack tips are sharp, i.e. that the tip radius is small. Figure 2 shows a typical example for defect 7. The photographs of all 6 surface breaking defect replicas are presented in Appendix 1. The opening angles range between 12º (defect 5) and 16º (defect 4).

	Length [mm]			Height [mm]			Through-Wall Extent [mm]		
No.	**Design**	**As built**	**Δ**	**Design**	**As built**	**Δ**	**Design**	**As built**	**Δ**
2	20.0	19.9	-0.1	5.0	5.0	0.0	5.0	5.0	0.0
3	20.0	20.0	0.0	5.0	5.0	0.0	5.0	5.0	0.0
4	30.0	40.0	10.0*	10.0	10.0	0.0	10.0	9.7	-0.3
5	30.0	40.0	10.0*	10.0	10.1	0.1	9.9	10.0	0.1
6	60.0	60.0	0.0	15.0	14.6	-0.4	14.9	14.5	-0.4
7	60.0	60.0	0.0	15.0	14.6	-0.4	14.5	13.6	-0.9

Table 2 – Measurements on surface defects

(*): A defect height-to-length ratio of ¼ was required due to the chosen defect fabrication technique. The departure from intended length sizes of defect 4 & 5 had no impact on the results of the pilot study.

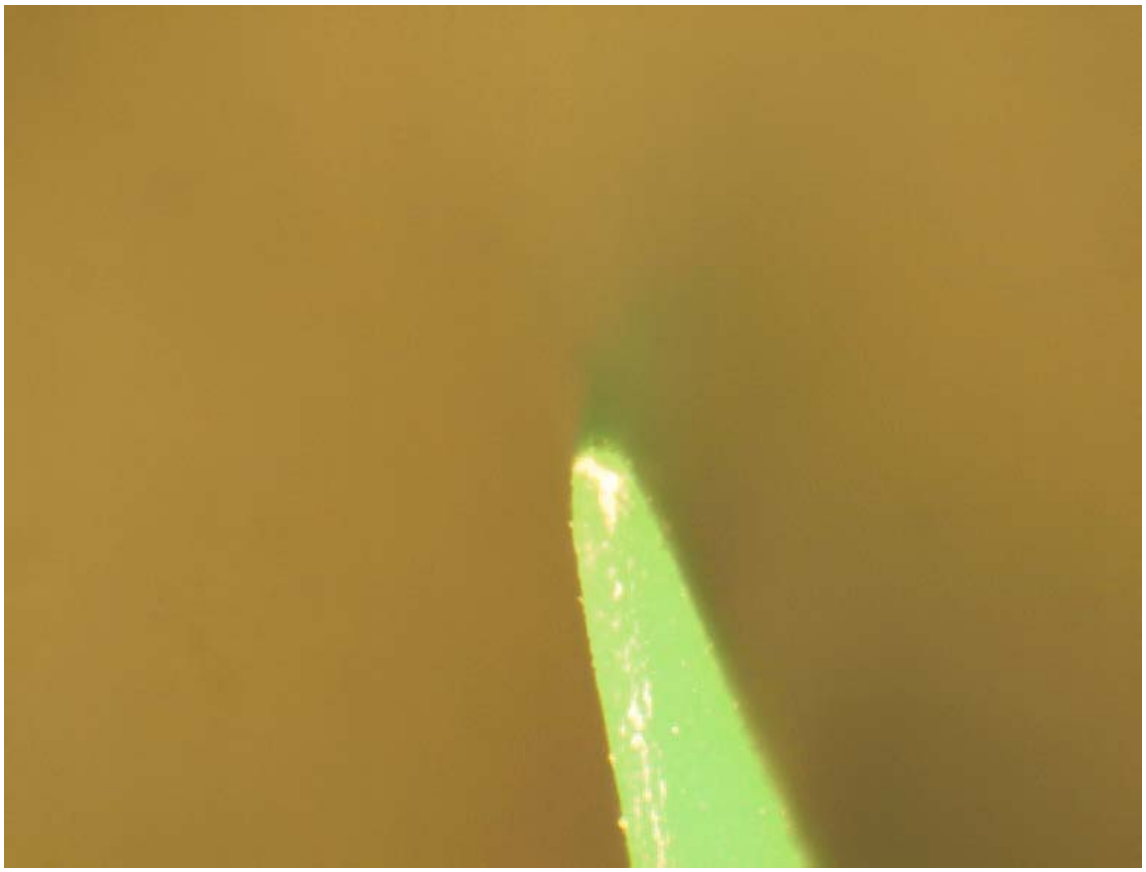

Figure 2 – Photograph of replica of defect 7

3.2 NEAR SURFACE DEFECTS

This section presents the result of the investigation of the near surface defects. All 6 defects, numbered 1 and from 8 to 12, were inserted by the same process as that used for the surface breaking defects. The near surface defects were surface-breaking prior to cladding and silica based replicas were taken on each defect, which were then investigated by the JRC, Institute for Energy in Petten.

Dimensions

Defect dimensions, length and height, in the pre-cladding state have been measured on the replicas under a microscope. The results are reported in Table 3, together with design data for the defects. The maximum departure from intended defect length and height sizes was found to be equal or less than 1.0 mm and 0.4 mm, respectively. The through-wall extent values in the pre-cladding state are reported as well, taken into account the effective tilt of the defects.

	Length [mm]			Height [mm]			Through-Wall Extent [mm]		
No.	**Design**	**As built(*)**	**Δ**	**Design**	**As built(*)**	**Δ**	**Design**	**As built(*)**	**Δ**
1	20.0	20.0	0.0	5.0	4.8	-0.2	5.0	4.8	-0.2
8	20.0	20.0	0.0	5.0	5.0	0.0	5.0	4.9	-0.1
9	40.0	39.5	-0.5	10.0	10.0	0.0	9.9	9.5	-0.4
10	40.0	39.0	-1.0	10.0	9.9	-0.1	9.4	8.4	-1.0
11	60.0	59.5	-0.5	15.0	14.6	-0.4	14.6	14.4	-0.2
12	60.0	59.5	-0.5	15.0	14.6	-0.4	14.9	14.6	-0.3

Table 3 – Measurements on near surface defects.

(*****): As built prior to cladding.

The application of the cladding layer, however, may have caused penetration through melting at the “shallow edge” of the defect facing the interface between base metal and cladding. This penetration may reduce the “as built” values. In order to avoid having melted cladding penetrating into the defect, wedges were placed in the openings of the then surface breaking defects before the cladding was applied (as illustrated in Figure 3, taken from another project).

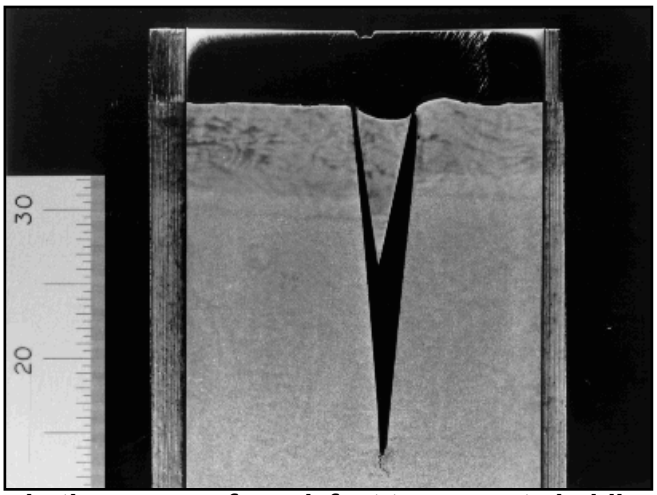

Figure 3 – Wedge in the near surface defect to prevent cladding penetration

As no destructive examination of the near surface defects has been performed, the effect of the cladding would have to be estimated based on experience. The Nuclear Research Institute (NRI) Řež has destructively examined the same type of near surface defects in other RPV components[9]. Welding experts have compared the NRI case with the ENIQ nozzle assembly 21 and estimated the penetration, based on materials and welding procedures used in the two cases. For the strip cladding used the estimated penetration is 1.5 mm.

According to previous experience obtained at JRC the penetration is maximum 1 mm, however no detailed comparison of materials and welding procedure have been made in this

case. For the near surface defects one would have to estimate the “as built” through-wall extent by reducing these values mentioned in Table 3 by 1 to 1.5 mm.

Crack tip geometry and opening angle

The investigation of replicas under microscope has confirmed that the crack tips are sharp, i.e. that the tip radius is small. Figure 4 shows a typical example for defect 1. The photographs of all near surface defect replicas (except for defect 8) are presented in Appendix 1. The opening angles range between 11º (defect 10) and 16º (defect 1).

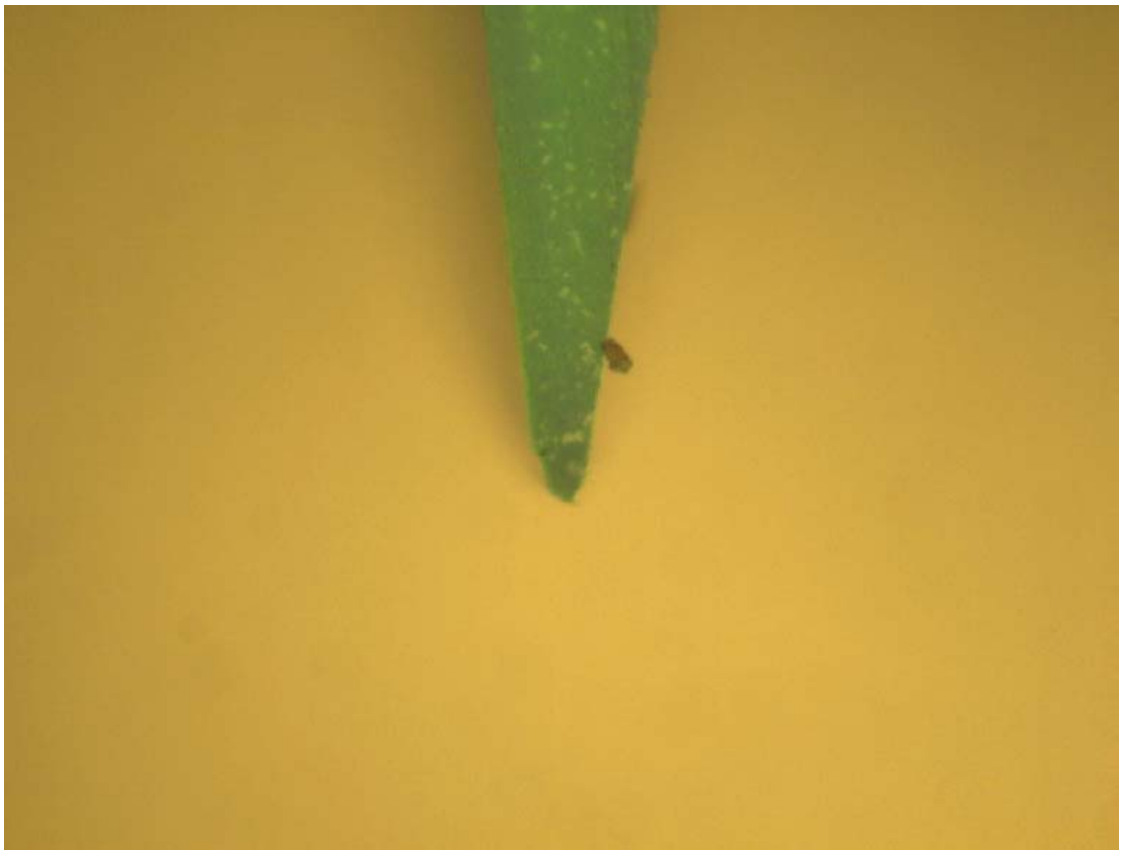

Figure 4 – Photograph of replica of defect 1

3.3 SIDEWALL LACK OF FUSION DEFECTS

This section presents the main result of the investigation of the sidewall lack of fusion defects. These 5 defects, numbered from 13 to 17, have been inserted by means of coupons, which were placed on the fusion faces. The sidewall lack of fusion defects were removed from the complete test piece by inserting spark erosion cuts in such a way as to produce smaller samples containing the defects. The defects were then sectioned at points along their length to reveal their dimensions, length and height, and the ligament to the inner clad surface. The orientation, peripheral position and weld preparation angle has been measured as well but is not reported in Table 4 (see Appendix 2 for more details). Three defects (No. 13, 16, 17) were selected for this work, which was done at the Nuclear Research Institute Řež.

	Length [mm]			Height [mm]			Ligament to Inner Surface [mm]		
No.	**Design**	**As built**	**Δ_{AVG}**	**Design**	**As built**	**Δ_{AVG}**	**Design**	**As built**	**Δ_{AVG}**
13	20.0	19.2 19.6	-0.4	10.0	11.49 11.08 10.30 10.90	0.94	10.0	10.88 10.97 11.20 10.90	0.98
16	50.0	48.4	-0.6	5.0	5.6 5.2 5.3 5.3	0.35	10.0	11.7 12.1 11.8 11.7	1.82
17	60.0	59.0 61.0	0.0	5.0	5.8 5.8 6.5 6.4	1.12	15.0	14.7 14.8 14.2 13.7	-0.65

Table 4 – Measurements on sidewall lack of fusion defects

Δ_{AVG} = (average "as built" value) – (design value)

It can be seen from the above that average defect length sizes were within 0.6 mm of those specified and average defect height sizes within 1.12 mm. Defect ligament for defect 16 was 1.82 mm different on average but the average discrepancy was less than 1.0 mm for the other two defects.

4. CONCLUDING REMARKS

Defect assessment and destructive examinations have been carried out to determine the true dimensions and orientations of the defects which were implanted in the ENIQ nozzle assembly 21. The "as built" values obtained by these investigations have been compared with the design values, and the departures have been considered sufficiently small for the purposes of the ENIQ 2nd Pilot Study.

For further information the reader is referred to the appendix and to the final report of the ENIQ 2nd Pilot Study[10].

REFERENCES

1 'European Methodology for Qualification of Non-Destructive Tests', EUR 17299 EN, 1997.

2 'Final Report of the First ENIQ Pilot Study', ENIQ Report No. 20, EUR 19026 EN, December 1999.

3 'Method of Working for the ENIQ 2nd Pilot Study', ENIQ Report ENIQ.TGQ (00), September 2002.

4 'Method of Working for the ENIQ 2nd Pilot Study – Issue 2', ENIQ Report ENIQ.TGQ (00), April 2005.

5 'Technical Justification for the ENIQ 2nd Pilot Study', ENIQ Report No. 26, EUR 22208 EN, December 2005.

6 'JRC ENIQ 2nd Pilot Study – Report for the Feasibility Study of the Procedure for the 2nd Pilot Study', WesDyne TRC AB Report R-T02-050, November 2002.

7 'JRC ENIQ 2nd Pilot Study – UT Inspection of Assembly 21 Performed from the Carbon Steel Side', WesDyne TRC AB Report R-T04-098, December 2004.

8 'ENIQ 2nd Pilot Study – Inspection Report for the Internal Inspection of the Clad Nozzle Assembly 21', ENIQ Report ENIQ.PILOT2 (05) 4, September 2005.

9 'Contribution to the Determination of the Penetration Depth in RPV A/C Claddings' – Report DITE 300/273, NRI Řež, December 2005.

10 'Final Report of the ENIQ 2nd Pilot Study', ENIQ Report No. 27, EUR 22539 EN, December 2006.

APPENDIX 1: Photographs of the silica based replicas of surface breaking and near surface defects

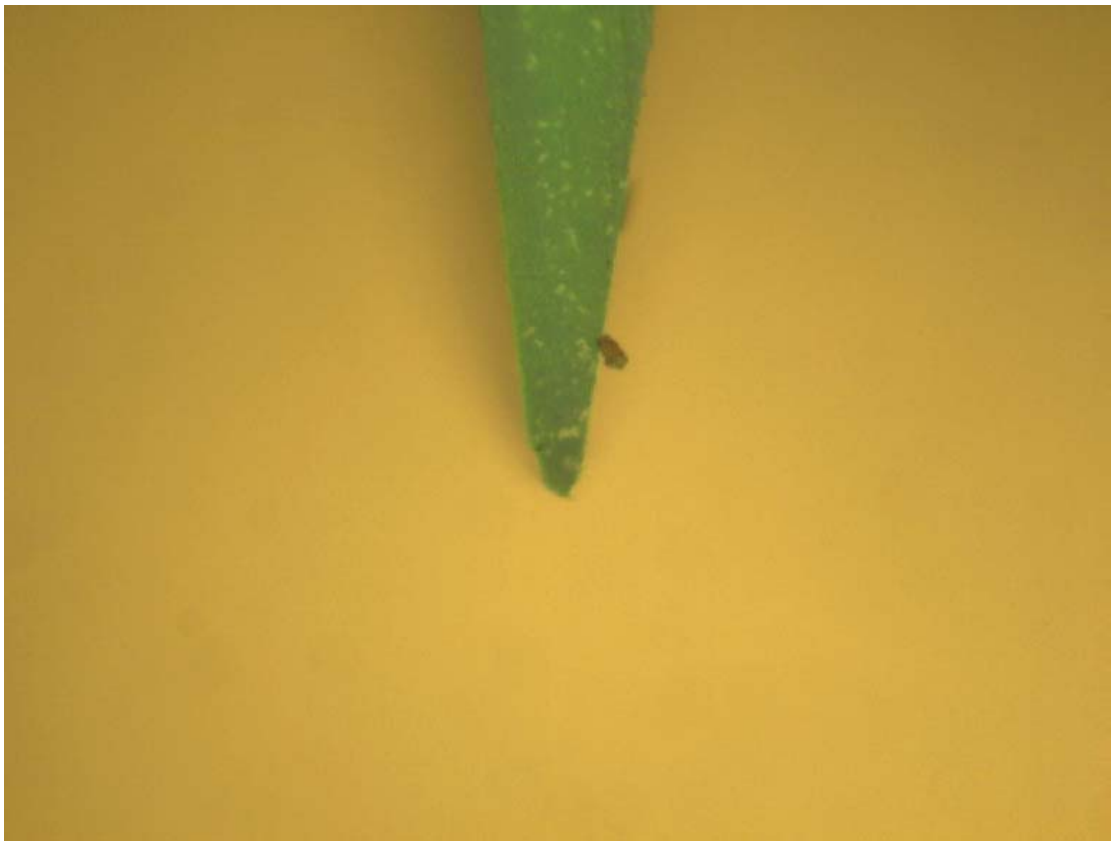

Figure 1 – Photograph of replica of defect 1

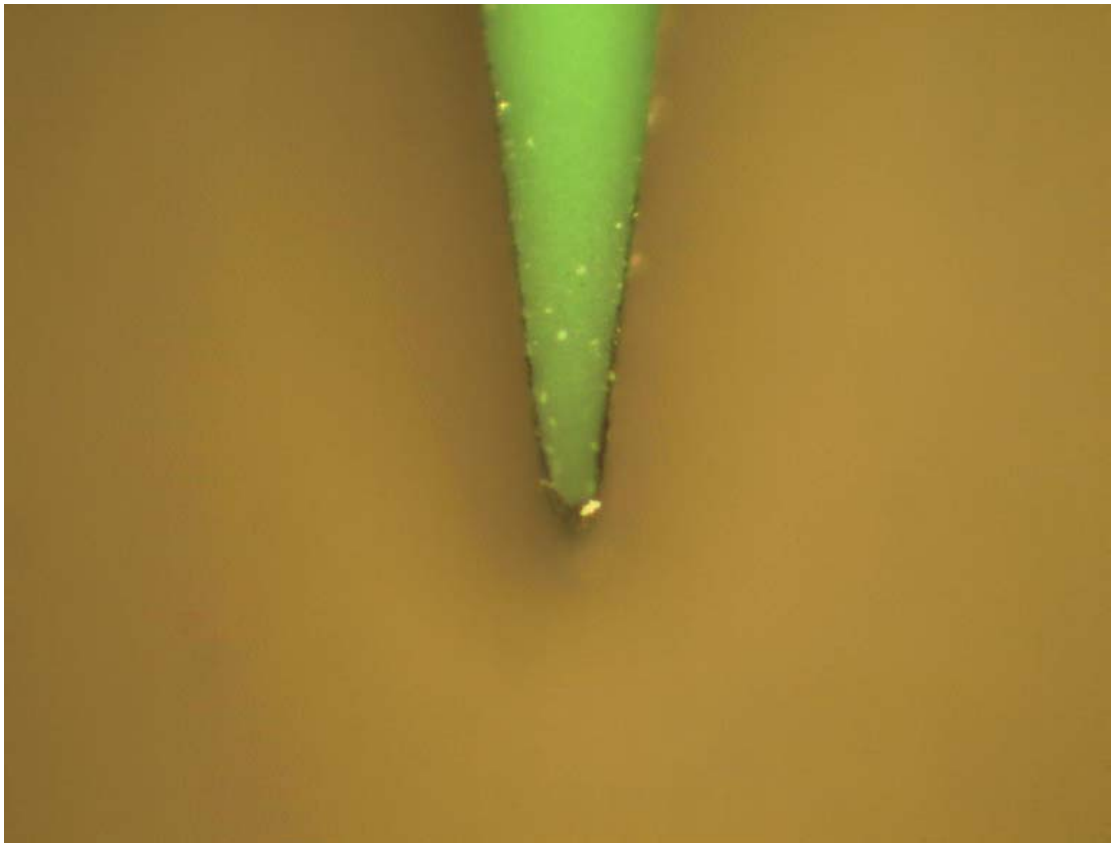

Figure 2 – Photograph of replica of defect 2

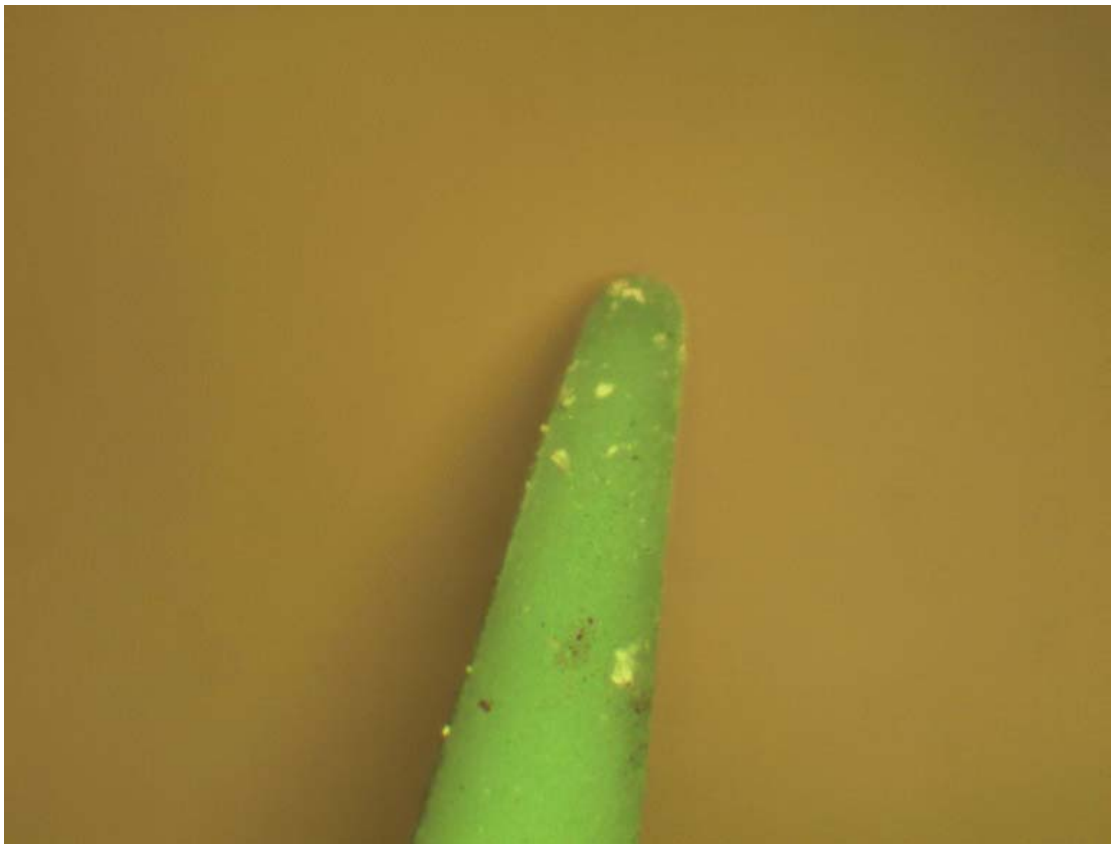

Figure 3 – Photograph of replica of defect 3

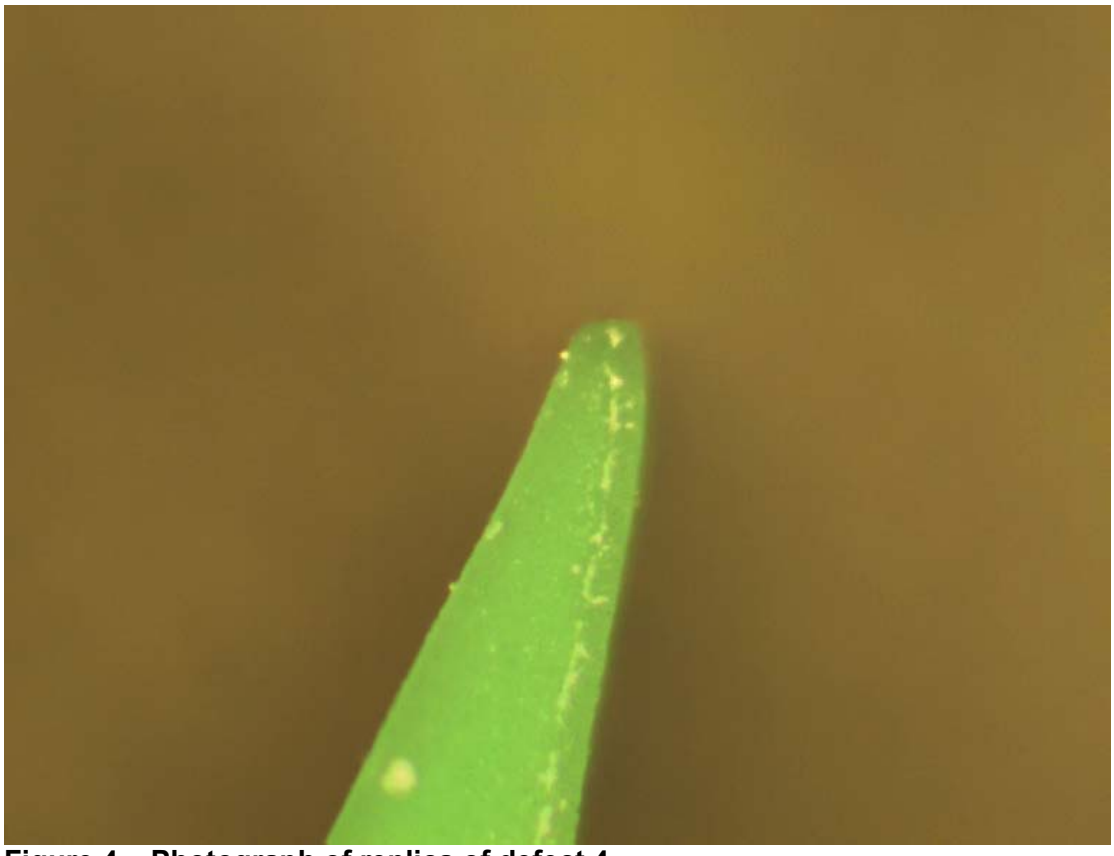

Figure 4 – Photograph of replica of defect 4

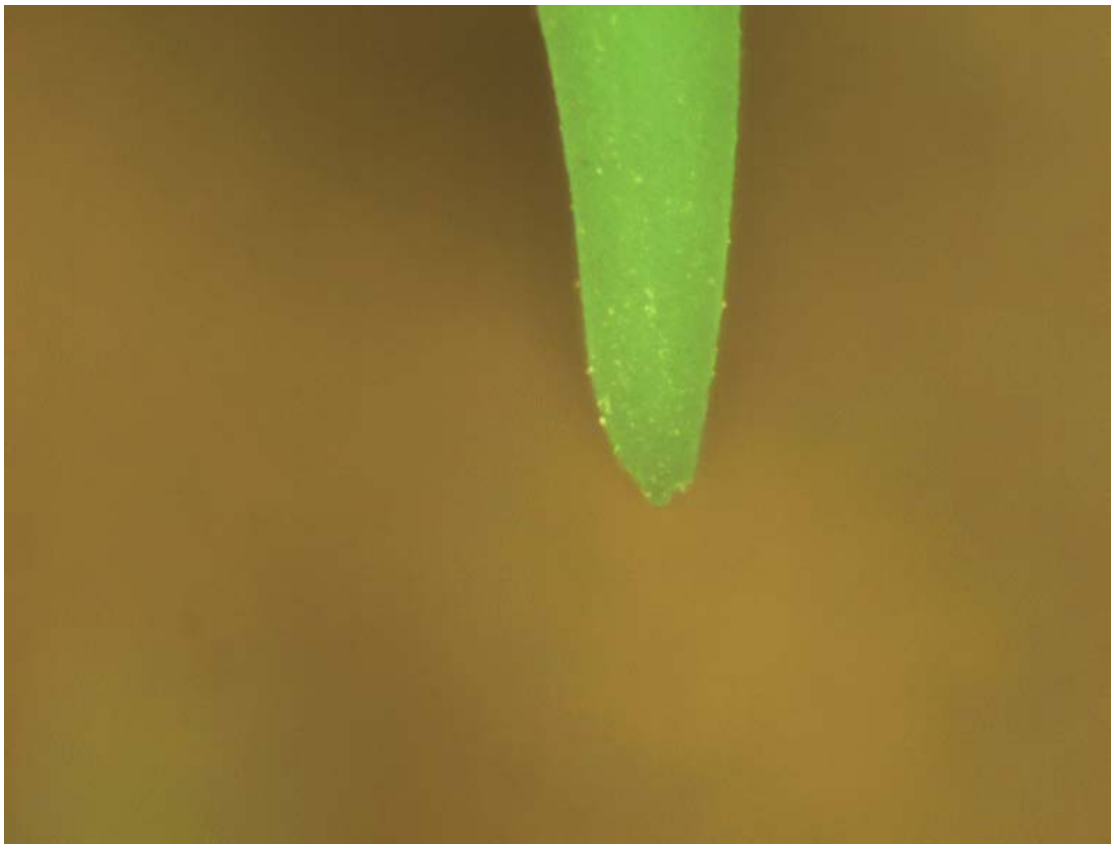

Figure 5 – Photograph of replica of defect 5

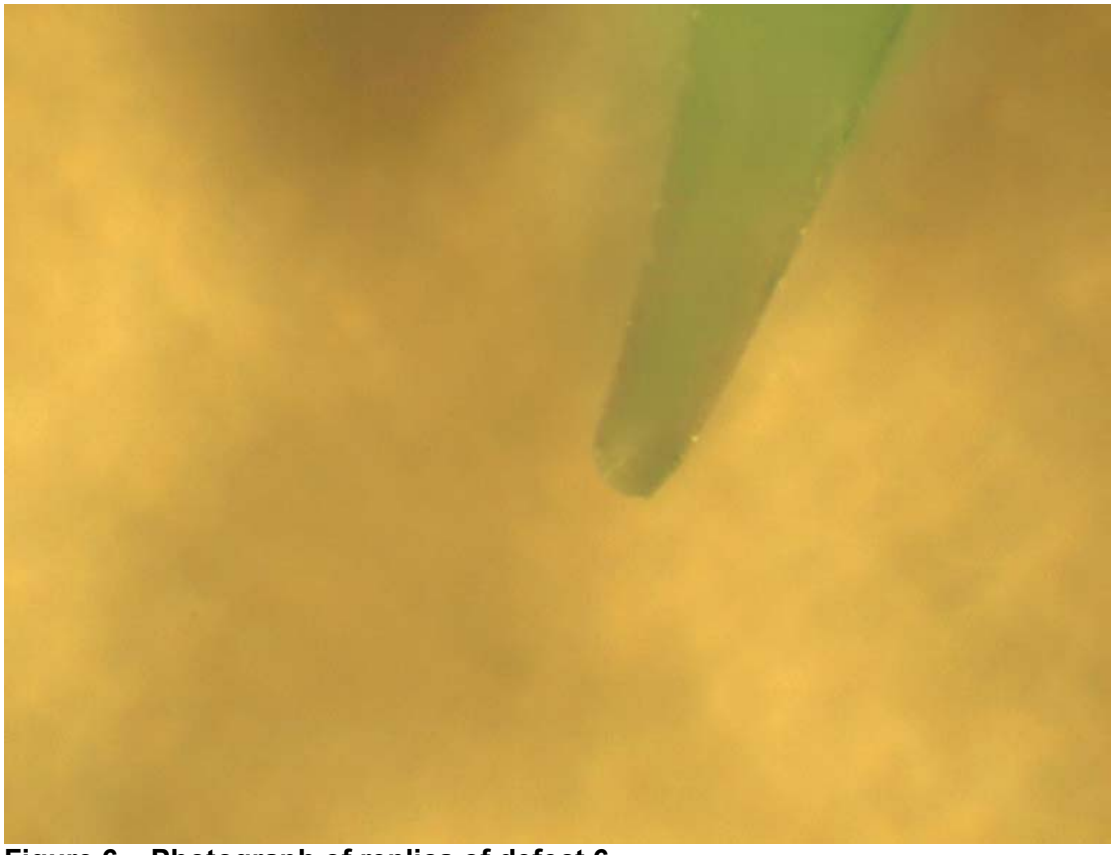

Figure 6 – Photograph of replica of defect 6

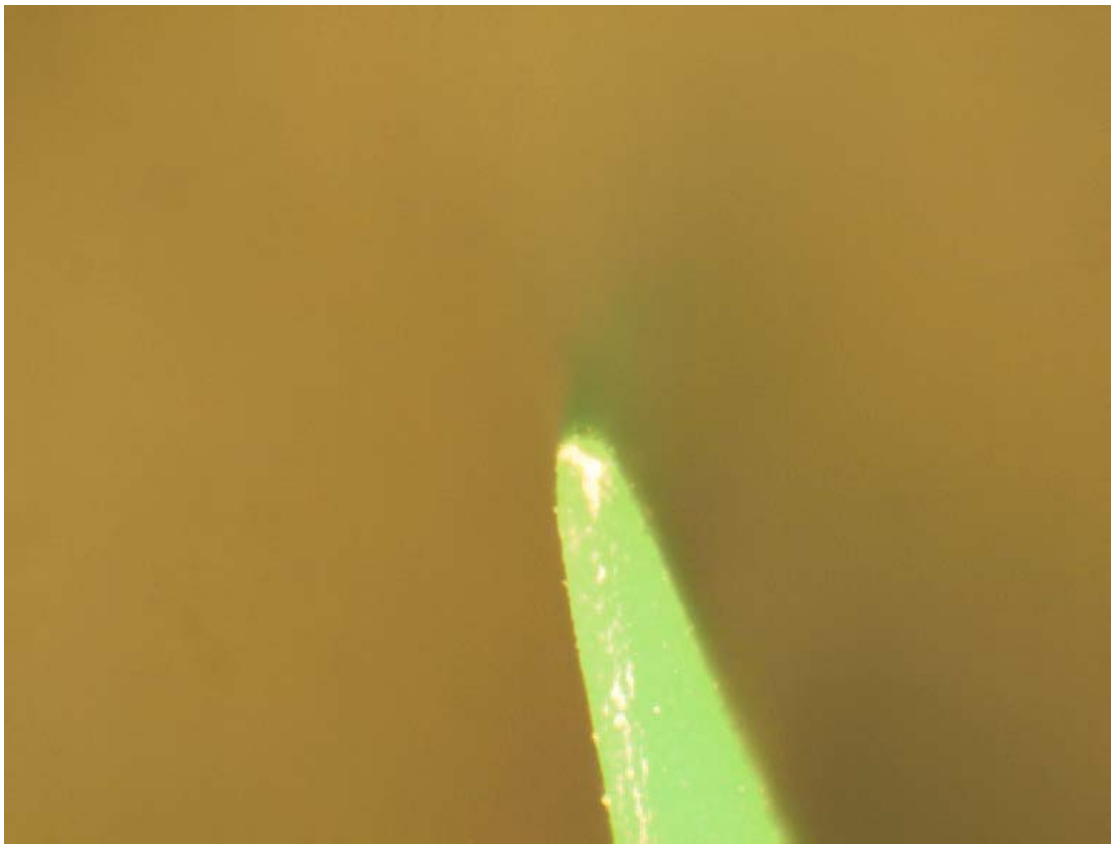

Figure 7 – Photograph of replica of defect 7

Figure 8 – Photograph of replica of defect 9

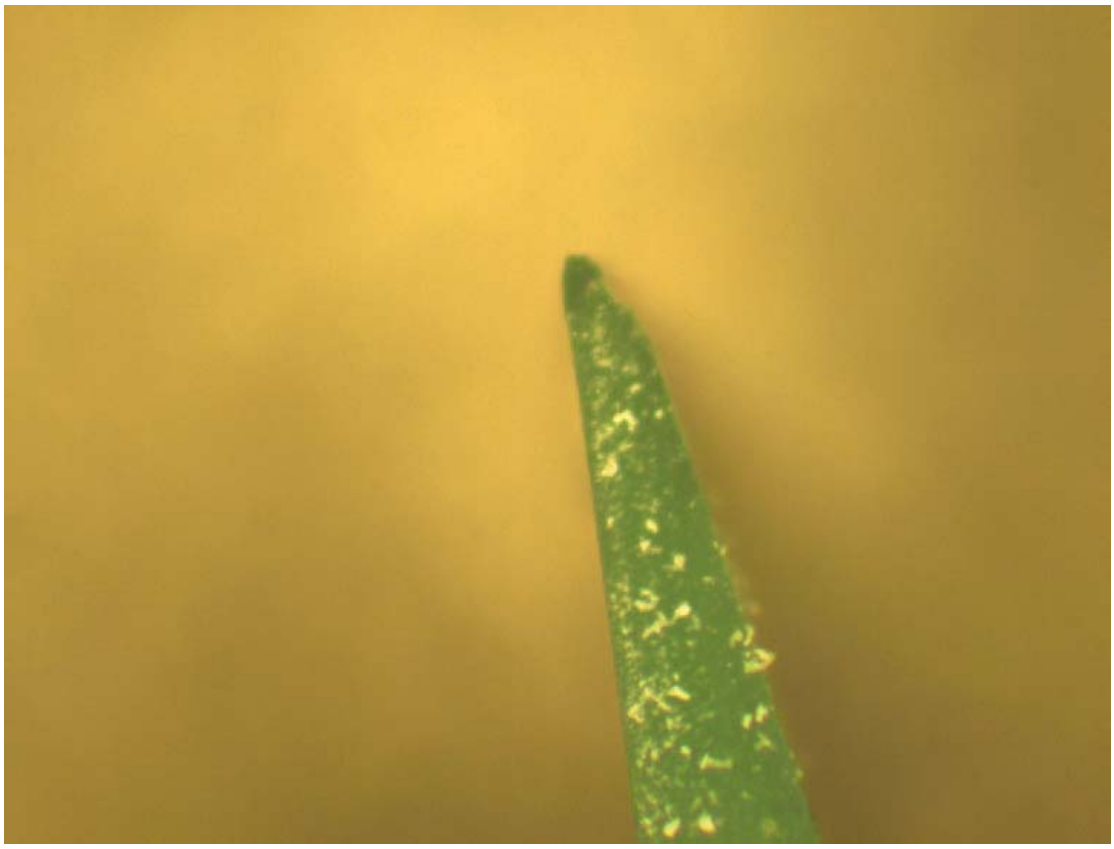

Figure 9 – Photograph of replica of defect 10

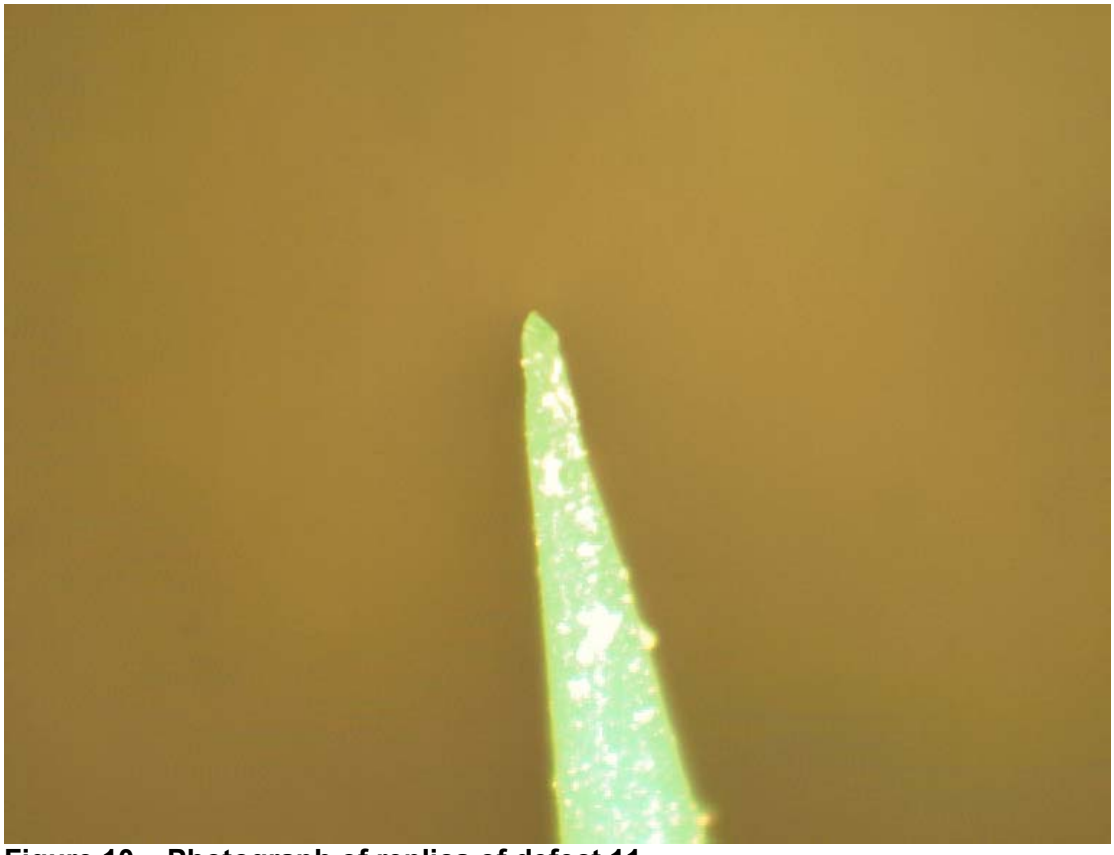

Figure 10 – Photograph of replica of defect 11

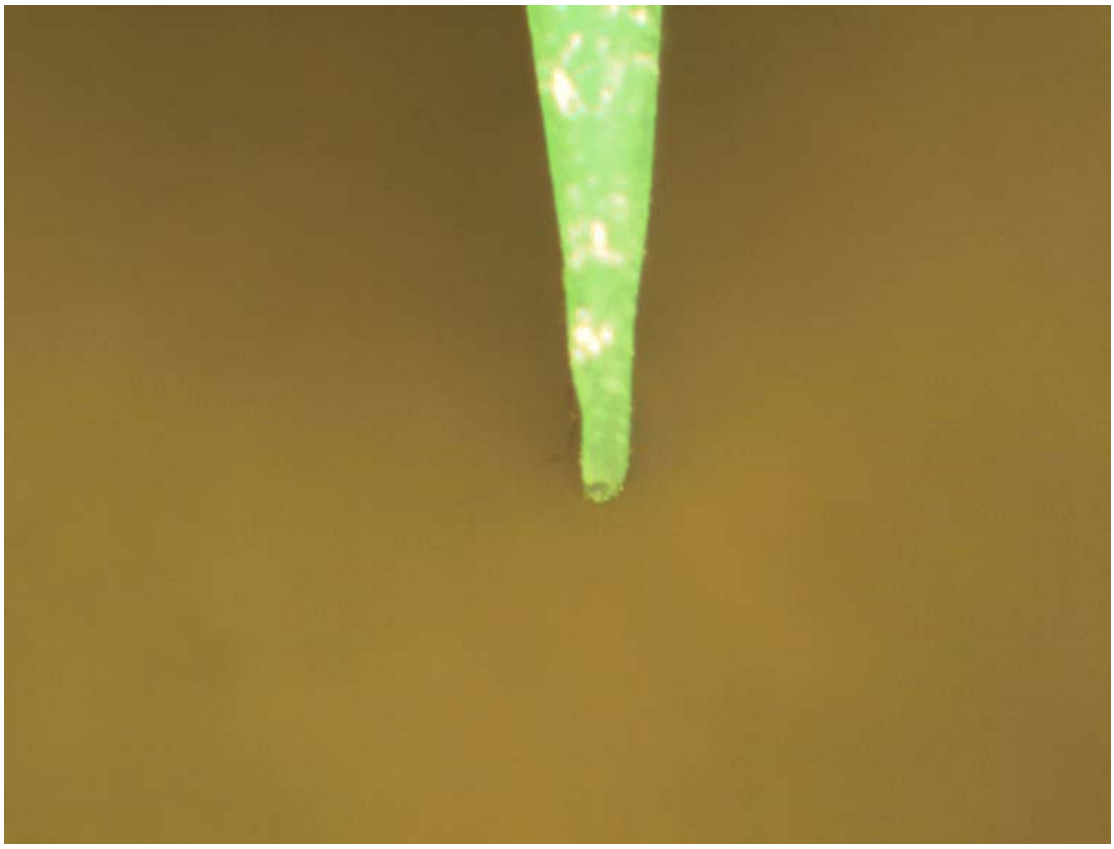

Figure 11 – Photograph of replica of defect 12

APPENDIX 2: NRI Řež report on the destructive examination of embedded defects 13, 16, 17

1. INTRODUCTION

This report summarizes results of the destructive examination of lack of fusion type of defects (LOFs) in N21 nozzle test assembly.
The LOFs are artificial types of defects of different sizes located at the boundary between ferritic weld metal and ferritic base metal along the weld bevels. The aim of this work was to determine defect parameters like position (through wall position, along the peripheral, ligament), size (height, length, width), skew, tilt and surface character) of three LOF type defects by the destructive examination.
Destructive examinations were done as a part of the ENIQ pilot study II project, in order to discuss and/or verify non-destructive examination and CIVA simulation results.
The chapter 2 contains summary of detailed information about the work procedure and equipment used during destructive examinations. EDM machine was used for cutting and light optical microscopy, metallography and image analyses were used for assessment and documentation of the destructive examination.
The chapters 3 – 5 contain description and results of the destructive examination of side wall LOF type defects No. 13, 16 and 17 respectively. There are presented descriptions and images of all sections and samples together with measured dimensions, positions and other required parameters of all three defects. Images of all three destructively examined defects with all examined sections are documented and included in appropriate Attachments (Attachment I-III). The chapter 6 contains metallographic description of the ferritic weld itself. Images of the N21 nozzle test block weld are included in Attachment IV.

2. WORK PROCEDURE AND USED EQUIPMENT

The decision to destructively examine these three defects was based on the agreement between JRC Petten and Nuclear Research Institute Řež, plc.
Three samples containing defects 13, 16 and 17 respectively have been cut out of the N21 BWR type nozzle test assembly. Each sample has been sectioned in two perpendicular planes so as to measure the exact above mentioned LOF defect type parameters directly on the individual section. If the section contained any other technological defect in the weld, caused by the defect manufacturing technology, it has been recorded as well. Every work step is documented on the photographs in the chapters 3 – 5.
The samples containing LOF type defects from the N21 test assembly were cut using electro-discharging machining (EDM) procedure in the mechanical workshop. The exact position of the cutouts has been determined in accordance with the 3D and 2D drawings of the test block. In order to avoid any possible mistake during manipulation, preparation or evaluation, each of the samples and their sections was assigned unique identification number according to the cutting plan.
In general all the samples and all their sections are marked in the same way for all three cutouts. At first the sections M1 and M4 have been prepared to determine the position of the ferritic weld and austenitic cladding. Then the main cutout has been cut into two samples AD and BC, see Fig. 2-1.

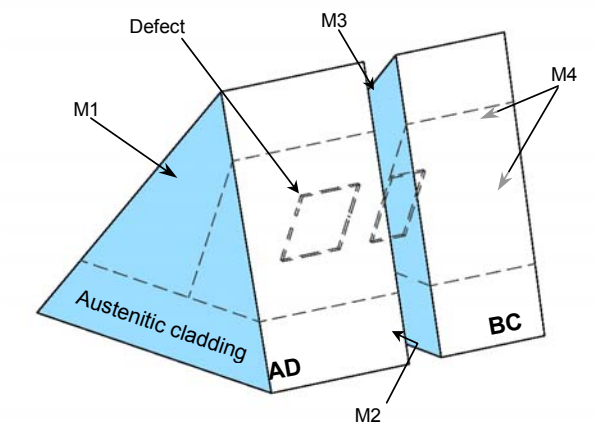

Fig. 2-1: Location of the sections after the first cut

The height and position of the LOF defect has been measured on sections M2 and M4. Then the sample AD has been cut into two samples A and D through the LOF defect. The partial length of the defect has been measured on both sections M7 and M8. The other sample BC has been cut in the same way; the defect partial length measured on both sections M5 and M6, see Fig. 2-2. When calculating the total defect length, the off cut of 2 mm was added to the values measured on both sections.

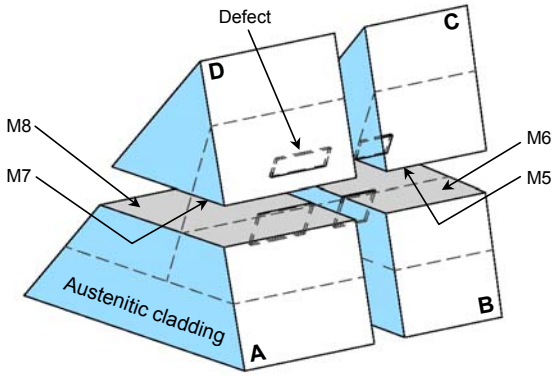

Fig. 2-2: Location of the sections after the second and third cut

In order to evaluate position of LOF defect with respect to the austenitic cladding, either the samples AD or BC have been cut through. The resulting sections M9-M12 allowed to verify the defect height, measured on sections M2 and M3 and also to check that the LOF defect is parallel with the austenitic cladding. Cutout 13 has been sectioned according to Fig. 2-3a; cutouts 16 and 17 according to Fig. 2-3b.

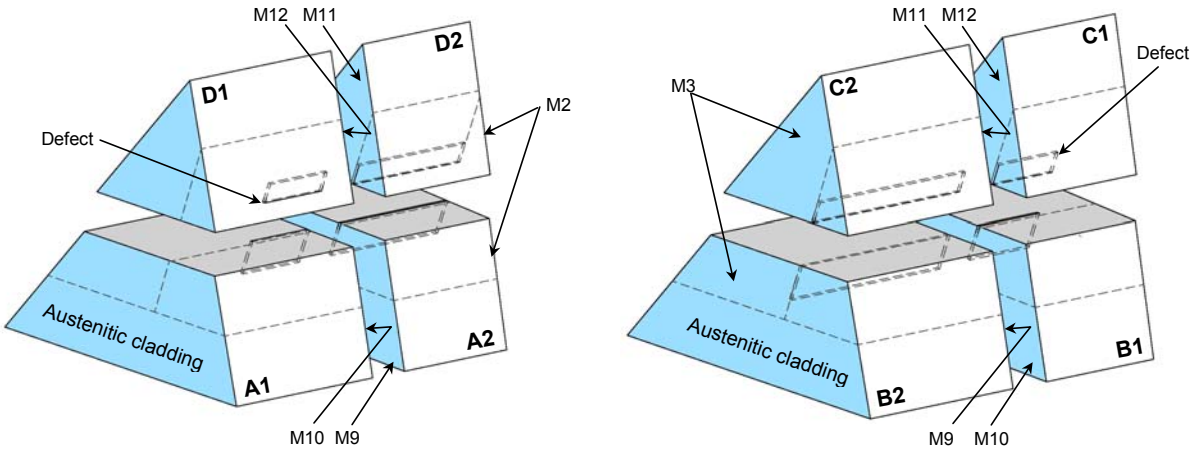

a) Sectioning of the cutout 13 *b) Sectioning of the cutouts 16 and 17*

Fig. 2-3: Location of the sections after the fourth and fifth cut

Each section was hand grinded (SiC papers 80 – 1000), polished (polishing cloth Struers, diamond suspensions 6 a 3 □m) and chemically etched in Nital solution (100 ml Methanol, 5 ml HNO3) for better weld visibility. Finished metallographical sections have been cleaned in ultrasonic bath in Methanol and dried in hot air stream to prevent staining.
At first the whole sample and the section area were documented using digital camera Nikon Coolpix 4500. Positions and dimensions of the artificial lack-of-fusion defects have been measured using image analyzer Lucia G connected to the light microscope Nikon Epiphot 300 (objectives 2,5x, 20x and 50x) with connected digital camera DVC. Measurement precision is 0,1 mm. Any other technological defects in the weld on the section area have been documented as well.

3. DEFECT NO. 13

3.1 DESTRUCTIVE EXAMINATION OF DEFECT NO. 13

The whole cutout with defect No. 13 is shown on Fig. 3-1a. Fig. 3-1c shows the cutout from the left side, section M4 is not yet polished. Top view of both sides shows position of the ferritic weld and austenitic cladding (sections M1 and M4, Fig. 3-1b and 3-1d). The sample was then cut into two parts 13AD and 13BC. The section M2 of the sample 13AD is shown on Fig. 3-2a. Metallographic documentation of the section is on Fig. 3-2cde. The plate, which is used as one part of the artificial defect, is clearly seen. Note the different morphology of both ends of the artificial defect resulting from slightly different fusion depth during welding. The bottom edge of the plate seen on Fig. 3-2e has likely not been thoroughly welded, resulting in small irregularity of the defect shape. However, the size of the affected area is less than 100 µm, and the resulting impact on NDT very small. Particles seen inside the defect crevice are residual burrs after cutting. No other defects have been found on the section M2.
The section M3 on the side of the sample 13BC is documented on the Fig. 3-3. Micrograph on Fig. 3-3c shows detail of the bottom end of the defect, where the weld beads have not been put properly. The resulting lack-of-fusion cavity is directly connected with the artificial defect. The position of the cavity corresponds with the irregularity on the facing section M2 – therefore it could be expected, that the axial length of the weld defect is higher than 2 mm. Maximum dimension of the cavity on the section M3 is 1x0.6 mm.

The sample 13A, cut out from the sample 13AD, is shown on Fig. 3-4a. The top view of the section M8, which has been used for measuring the artificial defect length, is shown on Fig. 3-4b. There are no other defects on the section surface.
The other part of the sample 13AD, sample 13D, is shown on Fig. 3-5a. The top view of the section M7 used for measurement of the defect length is shown on Fig. 3-5b.
The sample 13B, cut out from the sample 13BC, is shown on Fig. 3-6a. The top view of the section M6, which has been used to measure the artificial defect length, is shown on Fig. 3-6b. There are no other defects on the section surface.
The other part of the sample 13BC, sample 13C, is shown on Fig. 3-7b. This sample has been used for evaluation of the lack-of-fusion defect geometry in the corner. For this purpose one side of the sample has been machined away to see the exact defect shape. The top view of the section M5 used for measurement of the defect length is shown on Fig. 3-7a. Metallographic micrograph shows the defect position and shape in detail. Small irregularity on the defect end is caused by insufficient fusion of the inserted plate side. The dimensions of irregularity are small, about 100 x 200 μm.

In order to determine the height of the LOF defect on another section and also to check that the LOF defect is parallel with the austenitic cladding layer, another cut has been made. Both samples 13A and 13D have been cut through the LOF defect in parallel with section M2 and M3, see the drawing on Fig. 2-3a. The view of the LOF defect on the sections M9-M12 is seen on Fig. 3-7 and 3-8. There are no other technological defects on these sections.

The lack-of-fusion defect consists of two faces. One face surface is the area of the insert plate; the other is the area of the base metal. While the insert plate area is reasonably straight on the section, the base material side is slightly uneven, see Fig. 3-3c. In order to see the whole surface of the base metal, the insert plate and the surrounding weld beads were machined away, see Fig. 3-3f. The surface is covered with oxide layer, which is composed of Silicon oxides. This type of oxides could not be introduced into the crevice during sample preparation; in such a case they were without any doubt produced during welding process. The dimples, causing the uneven surface, are clearly seen.

The lack-of-fusion defect width at the tips is around 0,12 mm, and it gradually starts to increase up to 0,19 mm at the defect central position. The average defect width calculated from 20 measurement points is 0,15 mm.

3.2 DEFECT POSITION

The peripheral position of the defect No. 13 (left edge) is 257.4° (compared with the design value 257.0°). According to this comparison the circumferential shift of the defect No. 13 on the diameter of 746.8 mm is approximately 0.8 mm. Through-wall position of the defect No. 13 is measured as a ligament to the BM/cladding interface or to inner surface. The “as built” ligament of the defect to the BM/cladding interface of 2.56/3.08 mm corresponds to the design ligament value of 3 mm (see Tab. 3.1). Similarly the “as built” ligament of the defect to inner surface of 10.88/10.97 mm corresponds to the design ligament value of 11 mm (see Tab. 3.1). Position of the upper corner of the defect No. 13 is calculated in a similar way. The ligament of the lower bottom of the defect No. 13 to the BM/cladding interface is much more accurate than to the inner surface caused by the by scatter (much higher tolerance) of the cladding thickness than by the BM/cladding fusion line uncertainty.

Taking into account the above measurements the position of the defect No. 13 can be considered sufficiently accurate.

3.3 BEVEL (WELD PREPARATION) ANGLE

The sample cut out from Nozzle 21 also was used to determine the relative angle between the two weld fusion faces of the weld. Both fusion faces in the weld of the Nozzle test block N21 have according to the manufacturing drawing a nominal inclination angle of 4° (equal to the LOF type defect tilt) relative to the weld centre line, i.e. the nominal angle between bevels is 8°. During destructive examination this value was confirmed at the position of the LOF defect No.13, as follows:

- The bevel/tilt angle of 4° relative to the weld centre line can be measured and verified on appropriate sample by comparison of 3D CAD drawing of the Nozzle block 21 with a developed procedure for sample cut out using EDM electrodes (see Fig 3.3.1) and an “as built” value measured on the sample BC at section M3
- The bevel/tilt angle value determined on the sample BC at section M3 should be equal to the difference of two angles: 4° = 27° - 23° (see also Fig 3.3.1)
- The angle difference of the sample edges is 54.3°. It very well corresponds to the angle of 54° on Fig 3.3.1b
- Similarly the appropriate angles of values of 23° (see Fig 3.3.1b) and 24° differ only slightly on the level of fabrication/measurement tolerance (EDM machine, machining of sample).

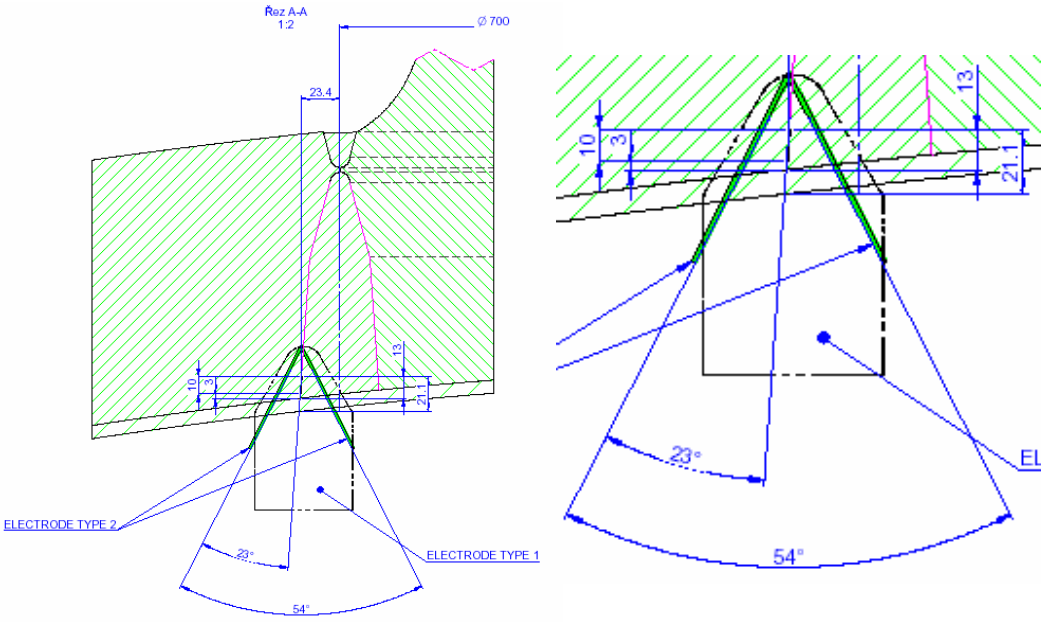

Fig. 3.3.1a – a general view

Fig. 3.3.1b – a detail view

Fig. 3.3.1 A part of the drawing for the defect No. 13 sample cut out by EDM machine

3.4 DEFECT HEIGHT

The height of the defect No. 13 measured at Section M2 (A-A) is 11.49 mm (Fig. 2.1) and at the opposite face of the cut (Section M3 or B-B) is 11.08 mm (see also Tab. 3.1). In any case due to the fact that the cut width is 2.0 mm after grinding and polishing, it is clear that the defect height is affected by the defect manufacturing technology and welding process penetration itself. Similarly the height of the defect No. 13 measured at Section M10 and M12 is 10.3 mm (5.3+1,9+3,5=10.3 mm, see Fig. 3.8b and Tab. 3.1) and at the opposite face of

the cut (at Sections M9 and M11) is equal to 10.9 mm (5.5+1.9+3.5 = 10.9 mm see Fig. 3-9b and also Tab. 3.1). Compared to the design defect height value of 10 mm the real height of defect No. 13 is slightly higher for about from 0.3 to 1.5 mm (see for summary Tab. 3.1).

3.5 DEFECT LENGTH

The length of the defect No.13 measured at two faces of the cut (at Sections M7 (C-C) and M5 resp. at Sections M8 (D-D) and M6) is 19.6 and 19.2 mm (see Fig. 3-4, 3-5, 3-6, 3-7). As the difference of “as built “ length compared with the design length of 20 mm is from 0.4 to 0.8 mm, the length of the defect No. 13 can be regarded as sufficiently precise (see also Tab. 3.1).

3.6 DEFECT WIDTH

The lack-of-fusion defect width at the tips is around 0.12 mm. It gradually starts to increase up to 0.19 mm at the defect central position. The average defect width calculated from 20 measurement points is 0.15 mm.

3.7 DEFECT TILT

Tilt of the defect No. 13 was verified to be equal 4° with the fabrication / measurement tolerance (EDM machine, machining of coupon segment). The procedure is described in 3.2.

3.8 DEFECT SKEW

Skew of the defect No. 13 was verified equal 0° with the fabrication / measurement tolerance (EDM machine, machining of coupon segment).

ŘEZ A-A

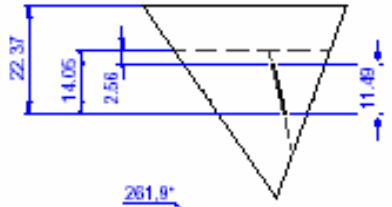

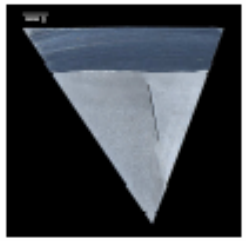

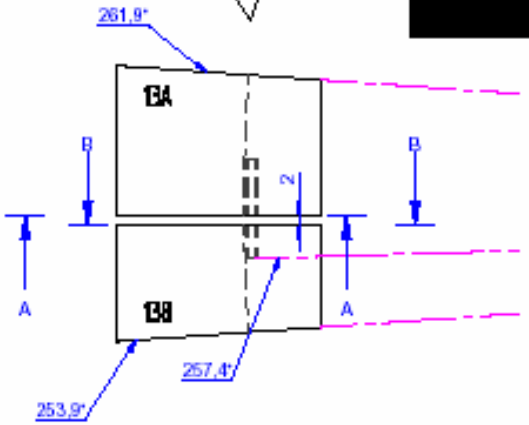

ŘEZ C-C

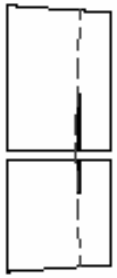

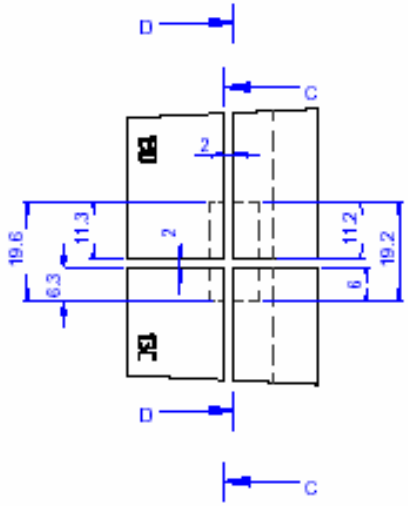

ŘEZ D-D

ŘEZ B-B

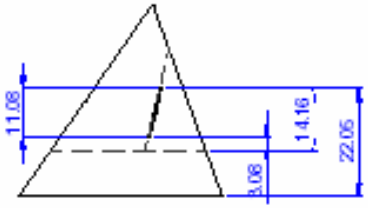

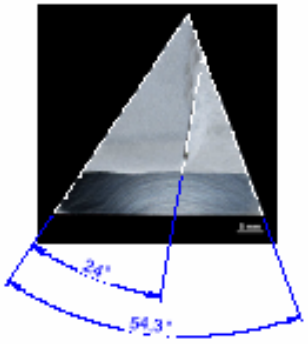

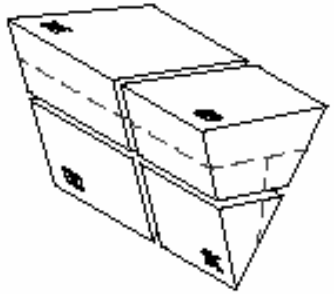

INDEX	CHANGE		DATE		NUCLEAR RESEARCH INSTITUTE Řež plc
MAT:	original:	SEMI:	dimension	GROSS WEIGHT:	1:1
	final:		standard	NET WEIGHT:	
DRAWN	LANDA 8.3.2006	STD. REF.		ASSEMBLY DRAW. NO.	
CHECKED				307-3-TNR DN250-0016-01	
TECHNOL.		APPROVED	Ing. Hordosk		
Name	TEST ASSEMBLY N21 DEFECT No.13			307-3-N21/13-BWR-001	
				SHEETS	SHEET

Table 3.1 – Through wall position and dimensions of defect No.13 in the ENIQ Nozzle Assembly 21

	Defect No. 13											
	Position				Distance of defect upper corner to				Dimensions			
	distance to BM / cladding interface		ligament to inner surface		BM/cladding interface		inner surface		defect height		defect length	
Sample / Section	design	as built	design	as built	design	as built	design	as built	design	as built	design	as built
	[mm]	[mm]	[mm]	[mm]	[mm]	[mm]	[mm]	[mm]	[mm]	[mm]	[mm]	[mm]
Sample AD Section M2	3	2,56	11	10,88	13	14,05	21	22,37	10	**11,49**		
Sample BC Section M3	3	3,08	11	10,97	13	14,16	21	22,05	10	11,08		
Sample A1D1 Sections M10, M12			11	11,2			21	21,5	10	10,3		
Sample A2D2 Sections M9, M11			11	10,9			21	21,8	10	10,9		
Samples A, B Sections M8, M6											20	19,2
Samples D, C Sections M7, M5											20	19,6

Table 3.2 – Peripheral position, orientation, tilt and skew of defect No.13 in the ENIQ Nozzle Assembly 21

	Defect No. 13									
	Position		Orientation						Weld preparation	
	pheripheral		fusion line to sample edge angle		tilt		skew		Bevels angle	
Sample / Section	design	as built	design	as built	design	as built	design	as built	design	as built
	[°]	[°]	[°]	[°]	[°]	[°]	[°]	[°]	[°]	[°]
Sample AD Section M2										
Sample BC Section M3			23	24	4	3,15	0	0	54	54,3
Sample A1D1 Sections M10, M12			23	24,7	4	2,65	0	0	54	54,7
Sample A2D2 Sections M9, M11			23	23,7	4	3,6	0	0	54	54,6
Side wall LOF defect	257	257,4								
Sample ABCD left edge	253,9	253,9								
Sample ABCD right edge	261,9	261,9								

4. DEFECT NO. 16

4.1 DESTRUCTIVE EXAMINATION OF DEFECT NO. 16

The whole cutout with the defect No. 16 is shown on Fig. 4-1a. Fig. 4-1c shows the cutout from the left side. Top view of both sides shows position of the ferritic weld and austenitic cladding (sections M1 and M4, Fig. 4-1b and 4-1d). Note several small technological defects close to the fusion line on the section M4. The heat-affected zone from the ferritic and austenitic weld is clearly visible as well.
The sample was then cut into two parts 16AD and 16BC. The section M2 of the sample 16AD is shown on Fig. 4-2a. Metallographic documentation of the section is on Fig. 4-2c-h. Several technological defects are seen on the section close to the LOF defect, see Fig 4-2a. The tips of the LOF defect itself are irregular, the bottom end shows improper fusion, the top end is accompanied by the pore. Two other technological defects are documented on Fig. 4-2fh. The first one is a lack-of-fusion defect, which is filled with oxides (see Fig. 4-2g taken with higher light intensity); the other one is a pore, which is not filled.
The section M3 of the sample 16BC is shown on Fig. 4-3. The technological defect inside the weld metal, see Fig. 4-3a, detail image on Fig. 4-3d, is likely continuation of the defect seen on the facing section M3. Technological defect close to LOF defect is documented on Fig. 4-3e; it is a pore type defect.
The sample 16AD was then cut into two parts 16A and 16D, see Fig. 4-4, the defect dimensions on both sections have been measured. There are no technological defects on these sections.
The sample 16BC has been cut in the middle of the LOF defect along the austenitic cladding. Section M6 of the sample 16B is shown on Fig. 4-5, the section M5 of the sample 16C is shown on Fig. 4-6. The defect tip on the section 16C is slightly irregular; see Fig. 4-6ce, result of improper welding along the insert plate. There is a small elongated technological defect inside the weld beads, see Fig. 4-6ad.
In order to determine the height of the LOF defect on another section and also to check that the LOF defect is parallel with the austenitic cladding layer, another cut has been made. Both samples 16B and 16C have been cut through the LOF defect in parallel with section M2 and M3, see the drawing on Fig. 2-3b. The view of the LOF defect on the sections M9-M12 is seen on Fig. 4-7 and 4-8. There is a technological defect on the section M12 – a pore in the weld beads, close to the base material. The pore maximum diameter is about 0,5 mm, it has not been detected on the facing section M11. There is a small irregularity in the defect tip, see detail on Fig. 4-7d, resulting from small error during welding along the insert plate.

4.2 DEFECT POSITION

The peripheral position of the defect No. 16 (left edge) is 324,5° (compared with the design value 324,0°). According to this comparison the circumferential shift of the defect No. 16 on the diameter of 653.8 mm is approximately 0.9 mm. Through-wall position of the defect No. 16 is measured as a ligament to the BM/cladding interface or to inner surface. The “as built” ligament of the defect to the BM/cladding interface of 1,8/2,6 mm corresponds to the design ligament value of 3 mm (see Tab. 4.1). Similarly the “as built” ligament of the defect to inner surface of 11,7/12.1 mm corresponds to the design ligament value of 11 mm (see Tab. 4.1). Position of the upper corner of the defect No. 16 is calculated in a similar way.
Taking into account the above measurements the position of the defect No. 16 can be considered sufficiently accurate.

4.3 BEVEL (WELD PREPARATION) ANGLE

The sample cut out from Nozzle 21 also was used to determine the relative angle between the two weld fusion faces of the weld. Both fusion faces in the weld of the Nozzle test block N21 have according to the manufacturing drawing a nominal inclination angle of 4° (equal to the LOF type defect tilt) relative to the weld centre line, i.e. the nominal angle between bevels is 8°. During destructive examination this value was confirmed at the position of the LOF defect No.16, as follows:

- The bevel/tilt angle of 4° relative to the weld centre line can be measured and verified on appropriate sample by comparison of 3D CAD drawing of the Nozzle block 21 with a developed procedure for sample cut out using EDM electrodes (see Fig 4.3.1) and an “as built” value measured on the sample BC at section M3
- The bevel/tilt angle value determined on the sample BC at section M3 should be equal to the difference of two angles: 4° = 27° - 23° (see also Fig 4.3.1)
- The angle difference of the sample edges is 53,8°. It very well corresponds to the angle of 54° on Fig 4.3.1b. The angle difference of the sample edges when measured on sections M10, M12 or M09, M11 is in both cases 55.9°.
- Similarly the appropriate angles of values of 23° (see Fig 4.3.1b) and 21,5° or similarly 21.1° (M10, M12) and 21.7° (M09, M11 - (see Tab. 4.1) differ only slightly on the level of fabrication/measurement tolerance (EDM machine, machining of sample).

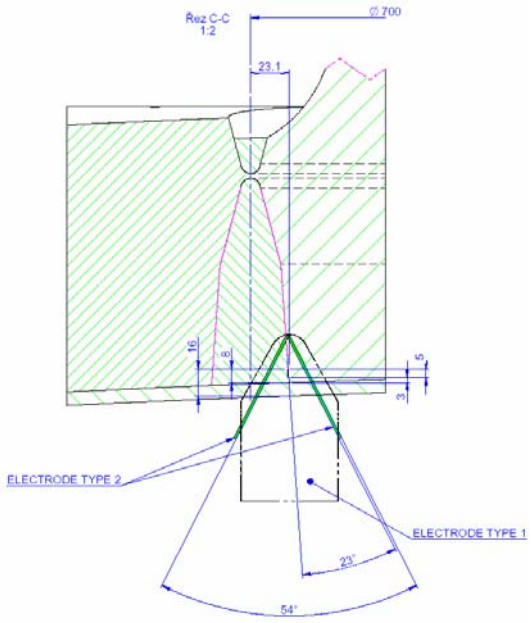

Fig. 4.3.1a – a general view

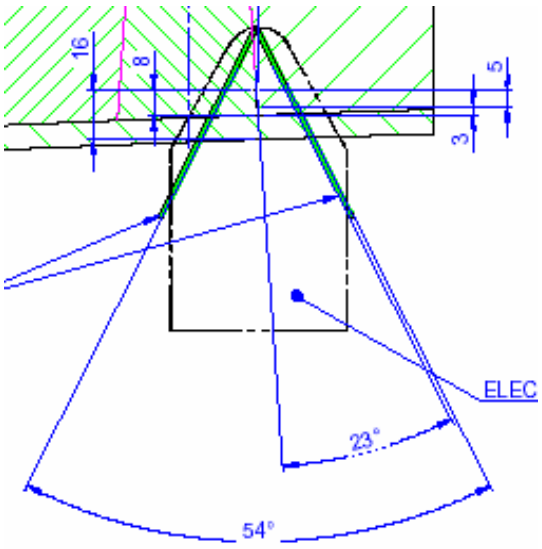

Fig. 4.3.1b – a detail view

Fig. 4.3.1 A part of the drawing for the defect No. 16 sample cut out by EDM machine

4.4 DEFECT HEIGHT

The height of the defect No. 16 measured at Section M2 (Section E-E) is 5,6 mm Fig. 2.1) and at the opposite face of the cut (Section M3 or F-F) is 5,2 mm (see also Tab. 4.1). In any case due to the fact that the cut width is 2.0 mm after grinding and polishing, it is clear that the defect height is affected by the defect manufacturing technology and welding process penetration itself. Similarly the height of the defect No. 16 measured at Section M10 and M12 is 5.3 mm (2.1+1.8+1.4 = 5.3 mm, see Fig. 4.8b and Tab. 4.1) and at the opposite face of the

cut (at Sections M9 and M11) is also equal to 5.3 mm (2.3+1.8+1.2 = 5.3 mm see also Tab. 4.1). Compared to the design defect height value of 5 mm the real height of defect No. 16 is slightly higher for about from 0.2 to 0.6 mm (see for the summary Tab. 4.1).

4.5 DEFECT LENGTH

The length of the defect No.16 measured at two faces of the cut (at Section M8 and M6) is 48.4 mm (see Fig. 4-4, 4-5, 4-6, and the drawing 307-3-N21/16-BWR-001). As the difference of “as built “ length compared with the design length of 50 mm is 1.6mm, the length of the defect No. 16 can be regarded as sufficiently precise (see also Tab. 4.1).

4.6 DEFECT WIDTH

Both surfaces of the LOF defect on all sections are almost straight; there are no areas of significant unevenness. The LOF defect width at the tips is around 0,06 mm, and it gradually starts to increase up to 0,12 mm at the defect central position. The average defect width measured in 15 points is 0,09 mm.

4.7 DEFECT TILT

Tilt of the defect No. 16 was verified to be equal 4+3 ° with the fabrication / measurement tolerance (EDM machine, machining of coupon segment). The procedure is described in 4.3.

4.8 DEFECT SKEW

Skew of the defect No. 16 was verified equal 0° with the fabrication / measurement tolerance (EDM machine, machining of coupon segment).

ŘEZ G-G

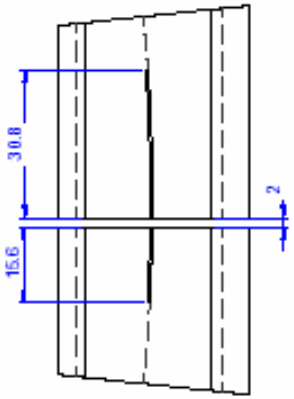

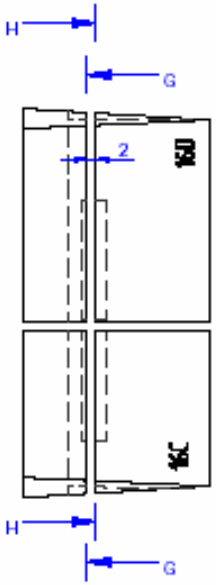

ŘEZ H-H

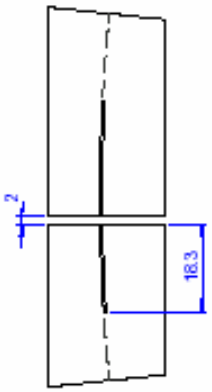

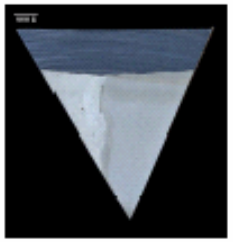

ŘEZ E-E

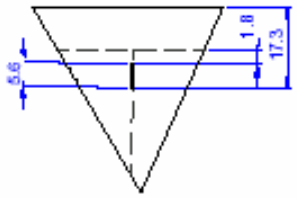

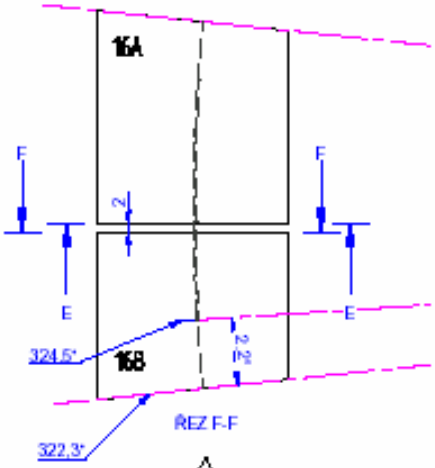

ŘEZ F-F

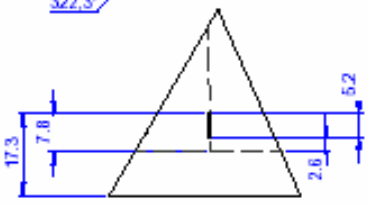

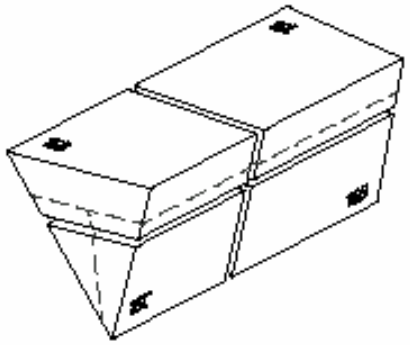

INDEX CHANGE		DATE	NUCLEAR RESEARCH INSTITUTE Řež plc
MAT: original / final	SEMI: dimension / standard	GROSS WEIGHT:	SCALE: 1:1
DRAWN LANDA 8.3.2006	STD. REF.	NET WEIGHT:	
CHECKED		ASSEMBLY DRAW. NO.	
TECHNOL.	APPROVED Ing. Hordesk	307-3-TNR DN250-0016-01	
Name: TEST ASSEMBLY N21 DEFECT No.16		307-3-N21/16-BWR-001	
		SHEETS	SHEET

Table 4.1 – Through wall position and dimensions of defect No.16 in the ENIQ Nozzle Assembly 21

Sample / Section	Defect No. 16											
	Position				Distance of defect upper corner to				Dimensions			
	distance to BM / cladding interface		ligament to inner surface		BM/cladding interface		inner surface		defect height		defect length	
	design	as built	design	as built	design	as built	design	as built	design	as built	design	as built
	[mm]	[mm]	[mm]	[mm]	[mm]	[mm]	[mm]	[mm]	[mm]	[mm]	[mm]	[mm]
Sample AD Section M2	3	1,8	11	11,7	8	7,4	16	17,3	5	5,6		
Sample BC Section M3	3	2,6	11	12,1	8	7,8	16	17,3	5	5,2		
Sample A1D1 Sections M10, M12			11	11,8			16	17,1	5	5,3		
Sample A2D2 Sections M9, M11			11	11,7			16	17	5	5,3		
Samples A, B Sections M8, M6											50	48,4
Samples D, C Sections M7, M5												

Table 4.2 – Peripheral position, orientation, tilt and skew of defect No.16 in the ENIQ Nozzle Assembly 21

Sample / Section	Defect No. 16									
	Position		Orientation						Weld preparation	
	pheripheral		fusion line to sample edge angle		tilt		skew		Bevels angle	
	design	as built	design	as built	design	as built	design	as built	design	as built
	[°]	[°]	[°]	[°]	[°]	[°]	[°]	[°]	[°]	[°]
Sample AD Section M2										
Sample BC Section M3			23	21,5	4	5,4	0	0	54	53,8
Sample A1D1 Sections M10, M12			23	21,7	4	6,25	0	0	54	55,9
Sample A2D2 Sections M9, M11			23	21,1	4	6,85	0	0	54	55,9
Side wall LOF defect	324	324,5								
Sample ABCD left edge	322,3	322,3								
Sample ABCD right edge	324,5	324,5								

5. DEFECT NO. 17

5.1 DESTRUCTIVE EXAMINATION OF DEFECT NO. 17

The whole cutout with defect 17 is shown on Fig. 5.1a. Fig. 5.1c shows the cutout from the left side. Top view of both sides shows position of the ferritic weld and austenitic cladding (sections M1 and M4, Fig. 5-1b and 5-1d). Note several small technological defects close to the fusion line. The heat-affected zone from the ferritic and austenitic weld is clearly visible as well.
The sample was then cut into two parts 17AD and 17BC. The section M2 of the sample 17AD is shown on Fig. 5-2a. Detail of slightly irregular LOF defect bottom is on Fig. 5-2c. The facing section M3 of the sample 17BC is documented on Fig. 5-3. No technological defects have been found on either section.

The sample 17AD has been cut through the LOF defect along the austenitic cladding. Section M8 of the sample 17A is shown on Fig. 5-4, facing section M7 of the sample 16D is shown on Fig. 5-5. Note bending of the LOF defect clearly seen on both sections. There are no technological defects in the weld metal. At one point (see arrows on Fig. 5-5a, detail Fig. 5-5c) the weld bead has significantly penetrated through the insert plate; less than 0,4 mm is left intact. This feature is not present on the facing section, its extend is limited.
The sample 17BC has been cut in the middle of the LOF defect along the austenitic cladding. Section M6 of the sample 17B is shown on Fig. 5-6, the section M5 of the sample 17C is shown on Fig. 5-7. There are no technological defects. The lack-of-fusion defect is formed from two surfaces. One surface is the area of the insert plate, the other is the area of the base metal. While the insert plate area is reasonably straight on the section, the base material side is slightly uneven, see Fig. 5-7cd.

In order to determine the height of the LOF defect on another section and also to check that the LOF defect is parallel with the austenitic cladding layer, another cut has been made. Both samples 17B and 17C have been cut through the LOF defect in parallel with section M2 and M3, see the drawing on Fig. 2-3b. The view of the LOF defect on the sections M10 and M12 is seen on Fig. 5-8, sections M9 and M11 are shown on Fig. 5-9. There is a technological defect on the section M11 and a pore in the weld metal, their positions and sizes are documented on Fig. 5-9c. An irregularity in the welding at the LOF defect bottom is shown on Fig. 5-9d.

5.2 DEFECT POSITION

The peripheral position of the defect No. 17 (left edge) is 350° (compared with the design value 350°). According to this comparison the circumferential shift of the defect No. 17 is negligible within the tolerance limit, approximately 0 mm. Through-wall position of the defect No. 17 is measured as a ligament to the BM/cladding interface or to inner surface. The “as built” ligament of the defect to the BM/cladding interface of 6/6.1 mm (6.1/5.7 mm) correspond to the design ligament value of 7 mm (see Tab. 5.1). Similarly the “as built” ligament of the defect to inner surface of 14.7/14.8 mm (14.2/13.7) correspond to the design ligament value of 15 mm (see Tab. 5.1). Position of the upper corner of the defect No. 17 is calculated in a similar way. Taking into account the above measurements the position of the defect No. 17 can be considered sufficiently accurate.

5.3 BEVEL (WELD PREPARATION) ANGLE

The coupons cut out from Nozzle 21 also has been used to determine the relative angle between the two weld fusion faces of the weld. The fusion faces in the weld of the Nozzle test block N21 have a nominal inclination angle of 4° relative to the weld centre line, i.e. the nominal relative angle between bevels is 8°. During destructive examination this value has been confirmed at the position of the LOF defect No.17, as follows:

- The nominal inclination of 4° relative to the weld centre line can be measured and verified on the coupon segment by comparison of 3D CAD drawing of the Nozzle block 21 with a developed procedure for coupon segment cut out using EDM electrodes (see Fig 5.2.1) and an “as built” value measured on the true coupon segment
- The nominal inclination value of 4° measured on the true coupon segment cut out (see Fig 5.2.1) should be equal to the difference of two angles: 4° = 27° - 23° (see Fig 5.2.1)
- The angle of the coupon segment edges is 53.3°, 55.4° (at Sections M10, M12), 55.3° (at Sections M09, M11). It corresponds to the angle of 54° on Fig 5.2.1b within expected tolerance.
- Similarly the appropriate angles of values of 23° (see Fig 5.2.1b) and 23,8° (or 25.3° (at Sections M10, M12), 25.6°(at Sections M09, M11) differ with the fabrication/measurement tolerance (EDM machine, machining of coupon segment).

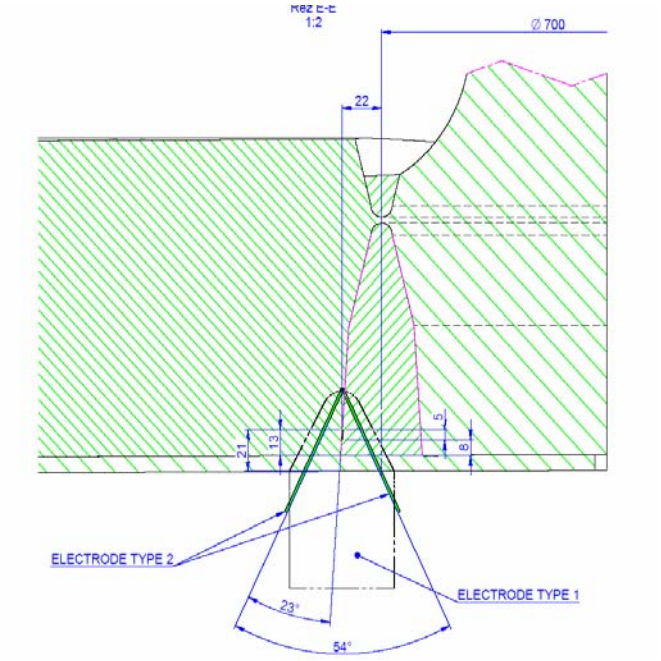

Fig. 5.3.1a – a general view

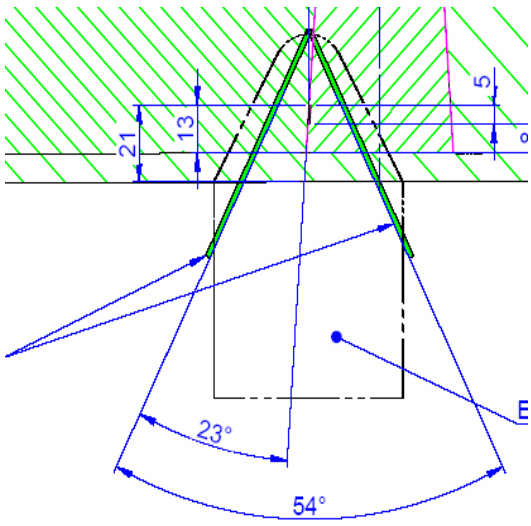

Fig. 5.3.1b – a detail view

Fig. 5.3.1 A part of the drawing for the defect No. 17 sample cut out by EDM machine

5.4 DEFECT HEIGHT

The height of the defect No. 17 measured at Section M2 (A-A) is 5.8 mm and at the opposite face of the cut (Section M3 B-B) is 5.8 mm (see also Tab. 5.1).

Similarly the height of the defect No. 17 measured at Section M10 and M12 is 6.5 mm (3.2+1.6+1.7) =6.5 mm, see Fig. 5.8b and Tab. 5.1) and at the opposite face of the cut (at Sections M9 and M11) is equal to 6.4 mm (3.5+1.6+1.3 = 6.4 mm see Fig. 5-9b and also Tab. 5.1). In any case due to the fact that the cut width is 2.0 (1.6) mm after grinding and polishing, it is clear that the defect height can change caused by size of the welding penetration into the defect (scatter of the defect surface fusion line). Compared to the design defect height value of 5 mm the real height of defect No. 17 is slightly higher for about from 0.8 to 1.5 mm (see for summary Tab. 5.1).

5.5 DEFECT LENGTH

The length of the defect No.17 measured at two faces of the cut (Sections M5 and M7 (D-D) resp. M6 and M8 (C-C) is 61 resp. 59 mm. As the difference compared with the design length of 60 mm is 1 mm, the length of the defect can be regarded as sufficiently precise (see Tab. 5.1).

5.6 DEFECT WIDTH

The lack-of-fusion defect width is very stable along the whole defect length. At the defect tip the width is around 0,06 mm, at the central position the width is 0,09 mm. The average defect width measured at 15 points is 0,07 mm.

5.7 DEFECT TILT

Tilt of the defect No. 17 has been verified to be equal 4-2 ° with the fabrication / measurement tolerance (EDM machine, machining of coupon segment). The procedure is described in 5.2.

5.8 DEFECT SKEW

Skew of the defect No. 17 has been verified to be equal 0° with the fabrication / measurement tolerance (EDM machine, machining of coupon segment).

ŘEZ A-A

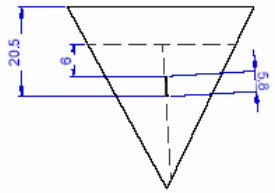

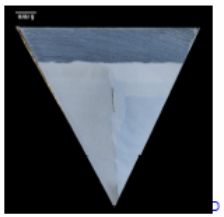

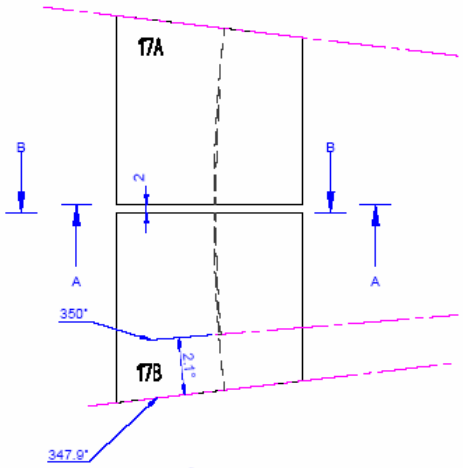

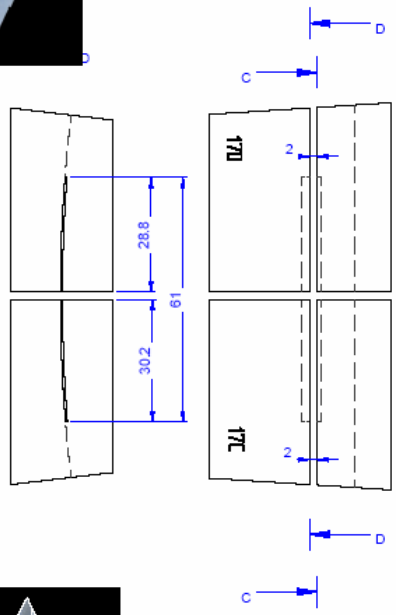

ŘEZ C-C

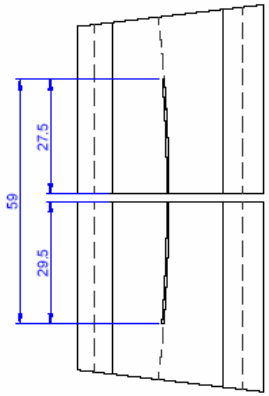

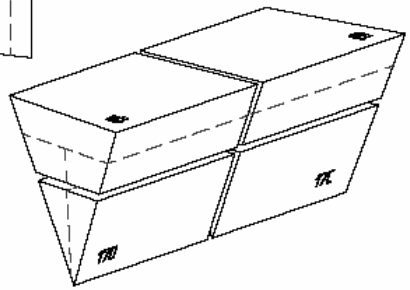

ŘEZ B-B

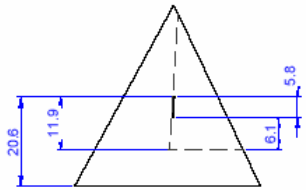

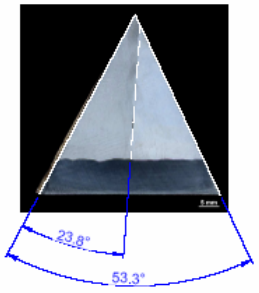

INDEX	CHANGE	DATE	SIGNATURE	NUCLEAR RESEARCH INSTITUTE Řež plc		
MAT. original:		SEMI dimension:		GROSS WEIGHT:	WASTE CLASS	SCALE: 1:1
final:		standard		NET WEIGHT:		
DRAWN LANDA 6.3.2006		STD. REF.		ASSEMBLY DRAW. NO.	POSITION	
CHECKED				307-3-TNR DN250-0016-01		
TECHNOL.		APPROVED Ing. Horáček				
Name: TEST ASSEMBLY N21 DEFECT No.17				307-3-N21/17-BWR-001		
				SHEETS SHEET		

Table 5.1 – Through wall position and dimensions of defect No.17 in the ENIQ Nozzle Assembly 21

Sample / Section	Defect No. 17											
	Position				Distance of defect upper corner to				Dimensions			
	distance to BM / cladding interface		ligament to inner surface		BM/cladding interface		inner surface		defect height		defect length	
	design	as built	design	as built	design	as built	design	as built	design	as built	design	as built
	[mm]	[mm]	[mm]	[mm]	[mm]	[mm]	[mm]	[mm]	[mm]	[mm]	[mm]	[mm]
Sample AD Section M2	7	6	15	14,7	12	11,8	20	20,5	5	5,8		
Sample BC Section M3	7	6,1	15	14,8	12	11,9	20	20,6	5	5,8		
Sample A1D1 Sections M10, M12	7	6,1	15	14,2	12	12,6	20	20,7	5	6,5		
Sample A2D2 Sections M9, M11	7	5,7	15	13,7	12	12,1	20	20,1	5	6,4		
Samples A, B Sections M8, M6											60	59
Samples D, C Sections M7, M5											60	61

Table 5.2 – Peripheral position, orientation, tilt and skew of defect No.17 in the ENIQ Nozzle Assembly 21

Sample / Section	Defect No. 17									
	Position		Orientation						Weld preparation	
	pheripheral		fusion line to sample edge angle		tilt		skew		Bevels angle	
	design	as built	design	as built	design	as built	design	as built	design	as built
	[°]	[°]	[°]	[°]	[°]	[°]	[°]	[°]	[°]	[°]
Sample AD Section M2										
Sample BC Section M3			23	23,8	4	2,85	0	0	54	53,3
Sample A1D1 Sections M10, M12			23	25,3	4	2,4	0	0	54	55,4
Sample A2D2 Sections M9, M11			23	25,6	4	2,05	0	0	54	55,3
Side wall LOF defect	350	350								
Sample ABCD left edge	347,9	347,9								
Sample ABCD right edge	361,5	361,5								

6. WELD MICROSTRUCTURE

The detailed microstructure has been documented on the section M2 of the sample 13AD. It has been selected as a typical example; all other sections exhibit similar microstructural features.

Microstructure of the multi-bead weld joint with artificially prepared lack-of-fusion defect is shown on Fig. 6-1a. The insert plate with thickness of more than 2 mm has been positioned on one side of the welded surface so that the crevice of about 0.25 mm is created. The multi-bead weld joint has been created using low-alloy filler material and later the austenitic cladding. During welding the insert plate has been partially melted, Fig. 6-1bcd, and both materials have been mixed. The weld beads, created from the filler material and from the mixing of the filler and insert material have different microstructure.

Microstructure of the filler weld material is typical for the low-alloy weld metals. The primary columnar austenitic grains with mixture of secondary structures (bainit, martensit, acicular ferrite, proeutectoid ferrite and likely also residual austenite, Figs. 6-1ab, 6-2b) are visible in the weld beads. Microstructure of the weld metal from mixture of the filler and insert plate material is homogenous; it is created by fine grain ferritic grain (approximately measured mean grain size 9 μm) with small particles precipitated along the grain boundaries, Fig. 6-1def.

The inserted plate has similar fine grain ferritic microstructure; the grain is somewhat more coarse (the mean size 13 □m) and the precipitation along the grain boundaries is less apparent, Fig. 6-2cd. However, this structure is not the original insert plate structure, because the material has been exposed to heat during welding (but not to the temperature of the phase transformation of mixing of materials).

The microstructure of the base material is also affected by heating during welding and corresponds with the heat-affected zone (HAZ), Fig. 6-2ef, Fig. 6-3b. The microstructure is ferritic, coarse grain (the mean grain size is 25 □m) with carbides precipitated along the grain boundaries. No material unaffected by any of the two welds has been available for metallographic examination.

The weld metal and base material directly under the austenitic cladding has smaller grain size and more homogenous structure, Fig. 6-3def.

Attachment I – Figures of Appendix 2 Chapter 3

Attachment II – Figures of Appendix 2 Chapter 4

Attachment III – Figures of Appendix 2 Chapter 5

Attachment IV – Figures of Appendix 2 Chapter 6

European Commission

EUR 22908 EN – DG JRC – Institute for Energy
ENIQ 2nd PILOT STUDY – DEFECT ASSESSMENT AND DESTRUCTIVE EXAMINATION REPORT

Authors

T. Seldis	DG-JRC-IE
A. Eriksson	DG-JRC-IE
M. Postler	NRI Řež
J. Landa	NRI Řež
P. Vomáčka	NRI Řež
D. Lisová	NRI Řež
E. Keilová	NRI Řež
J. Kohout	NRI Řež
L. Horáček	NRI Řež

Luxembourg: Office for Official Publications of the European Communities
2007 – 47 pp. – 21 x 29.7 cm
EUR - Scientific and Technical Research Series; ISSN 1018-5593

Abstract

This document compiles the results of the defect assessment and destructive examination carried out to determine the true dimensions and orientations of the defects, which have been deliberately implanted into the ENIQ nozzle assembly 21. Two different fabrication techniques have been used to implant the defects. Both surface breaking and near surface defects were produced by spark erosion using an electrode with a sharp tip. These are so-called PISC type A defects, and silica based replicas were taken on each defect after manufacturing. The silica based replicas were examined by the JRC, Institute for Energy in Petten. The second group of defects are located on the weld fusion faces and are embedded in the base material. These sidewall lack of fusion defects, which were produced by means of the so-called coupon technique, have been destructively examined by the Nuclear Research Institute (NRI) Řež.

The mission of the Joint Research Centre is to provide customer-driven scientific and technical support for the conception, development, implementation and monitoring of EU policies. As a service of the European Commission, the JRC functions as a reference centre of science and technology for the Union. Close to the policy-making process, it serves the common interest of the Member States, while being independent of special interests, whether private or national.

EUROPEAN COMMISSION
DIRECTORATE-GENERAL
Joint Research Centre

Publications Office
Publications.eu.int